HHS Public Access

Author manuscript

*Cell Rep*. Author manuscript; available in PMC 2024 September 25.

Published in final edited form as:

*Cell Rep*. 2024 August 27; 43(8): 114542. doi:10.1016/j.celrep.2024.114542.

# *Kmt2c* restricts G-CSF-driven HSC mobilization and granulocyte production in a methyltransferase-independent manner

**Helen C. Wang**[1,3], **Ran Chen**[1,3], **Wei Yang**[2], **Yanan Li**[1], **Rohini Muthukumar**[1], **Riddhi M. Patel**[1], **Emily B. Casey**[1], **Elisabeth Denby**[1], **Jeffrey A. Magee**[1,2,4,*]

[1]Department of Pediatrics, Division of Hematology and Oncology, Washington University School of Medicine, 660 S. Euclid Avenue, St. Louis, MO 63110, USA

[2]Department of Genetics, Washington University School of Medicine, 660 S. Euclid Avenue, St. Louis, MO 63110, USA

[3]These authors contributed equally

[4]Lead contact

## SUMMARY

Granulocyte colony-stimulating factor (G-CSF) is widely used to enhance myeloid recovery after chemotherapy and to mobilize hematopoietic stem cells (HSCs) for transplantation. Unfortunately, through the course of chemotherapy, cancer patients can acquire leukemogenic mutations that cause therapy-related myelodysplastic syndrome (MDS) or acute myeloid leukemia (AML). This raises the question of whether therapeutic G-CSF might potentiate therapy-related MDS/AML by disproportionately stimulating mutant HSCs and other myeloid progenitors. A common mutation in therapy-related MDS/AML involves chromosome 7 deletions that inactivate many tumor suppressor genes, including *KMT2C*. Here, we show that *Kmt2c* deletions hypersensitize murine HSCs and myeloid progenitors to G-CSF, as evidenced by increased HSC mobilization and enhanced granulocyte production from granulocyte-monocyte progenitors (GMPs). Furthermore, *Kmt2c* attenuates the G-CSF response independently from its SET methyltransferase function. Altogether, the data raise concerns that monosomy 7 can hypersensitize progenitors to G-CSF, such that clinical use of G-CSF may amplify the risk of therapy-related MDS/AML.

## In brief

Wang et al. show that *KMT2C* deletions, which occur commonly in therapy-related blood cancers, can hypersensitize hematopoietic stem cells to the cytokine G-CSF. *KMT2C* dampens



*Correspondence: mageej@wustl.edu.

AUTHOR CONTRIBUTIONS

J.A.M. designed and oversaw all experiments, conducted the experiments, interpreted the data, wrote the manuscript with H.C.W., and secured funding. H.C.W. and R.C. designed, conducted, and interpreted the experiments. W.Y. performed all bioinformatic analyses. R.M.P., E.B.C., E.D., Y.L., and R.M. performed the experiments and interpreted the data. All authors reviewed and edited the manuscript.

DECLARATION OF INTERESTS

The authors declare no competing interests.

SUPPLEMENTAL INFORMATION

Supplemental information can be found online at https://doi.org/10.1016/j.celrep.2024.114542.

G-CSF sensitivity independently from its histone methyltransferase activity. These observations have clinical implications, as G-CSF is widely used to accelerate hematopoietic recovery after chemotherapy.

## Graphical Abstract

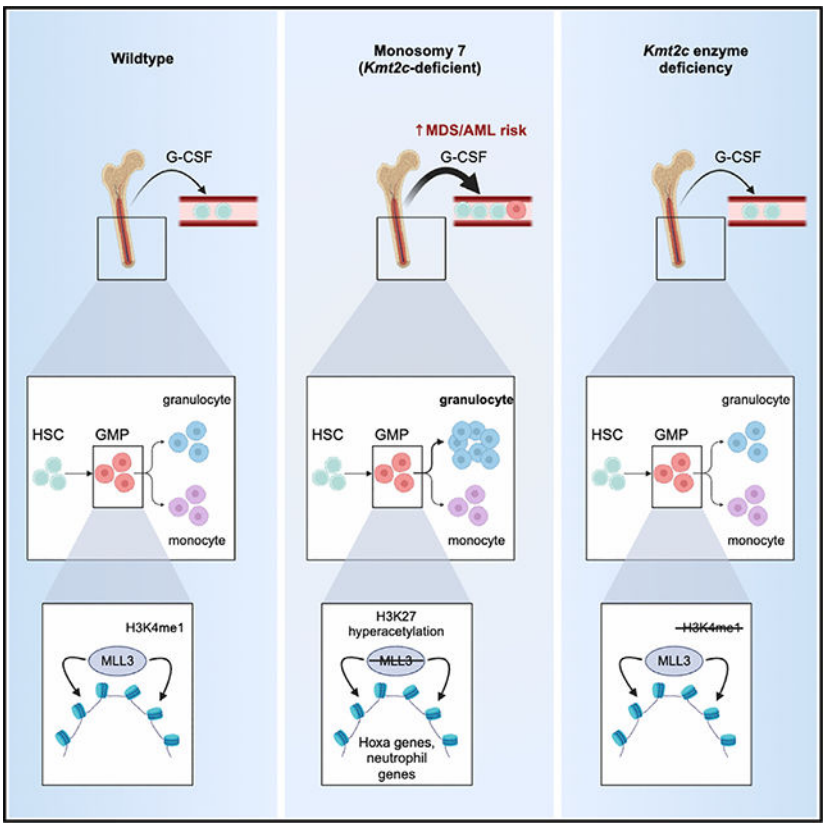


## INTRODUCTION

Granulocyte colony-stimulating factor (G-CSF) is a cytokine that stimulates myeloid cell production and hematopoietic stem cell (HSC) mobilization.[1–5] Pathogenic signals, such as bacterial lipopolysaccharide, stimulate stromal cells, endothelial cells, and macrophages to produce G-CSF, which then promotes myelopoiesis.[5–7] In addition, recombinant G-CSF is often used to accelerate neutrophil production after chemotherapy, to sustain neutrophil production in patients with inherited bone marrow failure such as severe congenital neutropenia (SCN),[8] and to mobilize HSCs for collection for autologous and allogeneic stem cell transplants.[4,9,10] G-CSF, therefore, has diverse roles in maintaining normal immune system homeostasis and enabling the effective management of cancer patients.

Use of recombinant G-CSF carries a potential risk that it will stimulate the growth of pre-leukemic progenitors, in addition to normal myeloid progenitors. This risk is well established in the setting of SCN, wherein ~80% of secondary AML patients acquire mutations that enhance signal transduction via the G-CSF receptor, CSF3R.[11,12]

A similar risk may apply when patients receive G-CSF to treat chemotherapy-induced neutropenia. Chemotherapy can both mutagenize HSCs and convey a selective advantage that predisposes to clonal hematopoiesis, therapy-related myelodysplastic syndrome (MDS), and/or acute myeloid leukemia (AML).[13] If certain mutations hypersensitize HSCs to G-CSF, then recombinant G-CSF could inadvertently amplify MDS/AML risk. Several recent studies have identified mutations that drive clonal hematopoiesis and MDS/AML after chemotherapy,[14–17] but it is not clear whether these mutations simultaneously sensitize hematopoietic progenitors to G-CSF.

Monosomy 7 is one of the most common genetic abnormalities found in both therapy-related and non-therapy-related MDS/AML.[18–20] *In vitro* studies have shown that monosomy 7 progenitors disproportionately expand when cultured with G-CSF,[21] although G-CSF does not appear to directly cause aneuploidy.[22] A case study has similarly demonstrated expansion of a monosomy 7 clone in a patient who received G-CSF to treat aplastic anemia. The mutant clone regressed following G-CSF termination.[23] The limited clinical data imply that G-CSF may drive the expansion of preexisting monosomy 7 clones, although it is not clear whether these observations generalize or which gene deletions might account for G-CSF hypersensitivity.

Monosomy 7 results in haploid deletion of many putative tumor suppressor genes, including *EZH2*, *KMT2C*, *LUC7L2*, *CUX1*, *KMT2E*, *DOCK4*, and *RASA4*.[19,24–27] Mouse modeling has confirmed critical roles for several of these genes in normal hematopoiesis and MDS/AML initiation. For example, *Cux1* suppression leads to an MDS-like illness,[28] and *Ezh2* deletions synergize with *Nras* mutations to promote AML in mice.[29] Large deletions of a region syntenic to 7q22 similarly lead to myeloid-biased HSC output that grows progressively more severe with age.[30] Finally, haploid *Kmt2c* deletions cooperate with *p53* and *Nf1* deletions to promote AML.[27] Interestingly, the majority of these mutations do not convey a selective advantage to HSCs, at least not as isolated haploid deletions. *Kmt2c* is an exception in that both heterozygous and homozygous deletions enhance HSC self-renewal.[31]

The *KMT2C* gene encodes an SET methyltransferase called MLL3 that monomethylates histone H3 at lysine 4 (H3K4me1).[32–34] MLL3 nucleates a large complex, called a COMPASS-like complex, that binds distal enhancers and potentiates gene expression via both methyltransferase-dependent and methyltransferase-independent mechanisms.[35–37] MLL3-bound chromatin regions often demonstrate high levels of histone H3, lysine 27 acetylation (H3K27ac) that is achieved through the recruitment of p300/CBP histone acetyltransferase,[38] although H3K27ac placement can occur independently from MLL3 methyltransferase activity.[35] These observations implicate *KMT2C*/MLL3 as a critical epigenetic regulator that is frequently mutated in the context of monosomy 7 MDS/AML.

We previously characterized the role of *Kmt2c* in HSC maintenance during native hematopoiesis and under stress conditions that included transplantation, chemotherapy treatment, and inflammation.[31] Under steady-state conditions, mono- and biallelic *Kmt2c* deletions led to modest expansion of the HSC pool at the expense of multipotent progenitors (MPPs). In contrast, *Kmt2c* deletions conveyed a profound competitive advantage to HSCs in serial transplantation assays and after chemotherapy. Loss of *Kmt2c*/MLL3 prevented

the efficient activation of genes that promote HSC to MPP differentiation, and it impaired HSC differentiation in response to the inflammatory cytokine interleukin-1β (IL-1β). These observations support a model wherein *KMT2C* haploinsufficiency (due to acquired monosomy 7) conveys a selective advantage to HSCs as they cycle to regenerate the hematopoietic system after chemotherapy. This advantage ultimately predisposes to therapy-related MDS/AML.[31] The model raises the question of whether G-CSF further exacerbates the expansion or mobilization of *Kmt2c*-deficient HSCs, given that G-CSF is incorporated into many supportive care regimens.

In this study, we used conditional loss-of-function mice and cellular indexing of transcripts and epitopes by sequencing (CITE-seq) to test whether *Kmt2c* deletions sensitize HSC and myeloid progenitors to G-CSF. Loss of just a single *Kmt2c* allele enhanced the mobilization of HSCs, pre-granulocyte-monocyte progenitors (pGMs) and granulocyte-monocyte progenitors (GMPs). CITE-seq showed that *Kmt2c*-deficient HSCs have reduced the expression of several adhesion molecules that are known to restrict mobilization and help HSCs remain in the bone marrow. *Kmt2c* deficiency also greatly amplified granulocyte production from G-CSF-stimulated GMPs. Interestingly, *Kmt2c*-deficient, G-CSF-stimulated GMPs demonstrated higher rather than lower levels of H3K27ac at genes associated with self-renewal (e.g., *Hoxa* genes) and neutrophil differentiation. H3K4me1 patterns offered little insight into why *Kmt2c* deficiency would amplify granulocyte production, and the finding suggested that *Kmt2c*/MLL3 may instead regulate hematopoietic fate primarily via methyltransferase-independent mechanisms. We generated mice with a point mutation that disables the MLL3 SET domain (Y4793A)[35,37] and confirmed that several key *Kmt2c*/MLL3 activities in the hematopoietic system, including restrictions on HSC-repopulating activity, HSC mobilization and G-CSF-stimulated granulocyte production, all are methyltransferase independent.

Together, our data show that *Kmt2c* mutations can enhance HSC mobilization and myelopoiesis in response to G-CSF via methyltransferase-independent mechanisms. This finding raises concerns that acquired *KMT2C* haploinsufficiency, through the loss of chromosome 7, could convey a selective advantage to pre-leukemic HSCs that is then amplified by therapeutic G-CSF. This interaction has implications for autologous transplants, as G-CSF-stimulated HSC mobilization could disproportionately enrich for monosomy 7 progenitors and exacerbate the risk for t-MDS/AML.

## RESULTS

### *Kmt2c* deletions enhance myelopoiesis and HSC mobilization in response to G-CSF

We used conditional loss-of-function mice to test whether *Kmt2c* deletions enhance progenitor mobilization in response to G-CSF. We treated $Cre^-$ control, $Kmt2c^{f/+}$; *Vav1-Cre* ($Kmt2c^{\Delta/+}$), and $Kmt2c^{f/f}$; *Vav1-Cre* ($Kmt2c^{\Delta/\Delta}$) young adult mice with vehicle (PBS) or G-CSF (5 μg/dose) subcutaneously for 4 days.[3,39] We then measured peripheral blood counts and various hematopoietic progenitor populations in the blood, spleen, and bone marrow. Peripheral white blood cell (WBC) numbers and absolute neutrophil counts (ANC) were significantly elevated in $Kmt2c^{\Delta/+}$ and $Kmt2c^{\Delta/\Delta}$ mice relative to $Cre^-$ controls (Figures 1A and 1B). Differences in WBC and ANC levels were not

observed among the *Kmt2c* genotypes in vehicle-treated mice. Colony-forming units (CFU) were elevated in the blood of $Kmt2c^{\Delta/\Delta}$ mice relative to controls (Figure 1C), as were blood and spleen HSC ($CD150^{+}CD48^{-}Lineage^{-}Sca1^{+}Kit^{+}$), MPP3/4 ($CD150^{-}CD48^{+}Lineage^{-}Sca1^{+}Kit^{+}$), pGM ($CD150^{-}CD105^{-}CD16/32^{-}Lineage^{-}Sca1^{-}Kit^{+}$) and GMP ($CD150^{-}CD105^{-}CD16/32^{+}Lineage^{-}Sca1^{-}Kit^{+}$) numbers (Figures 1D–1I), based on previously described surface marker phenotypes (Figure S1).[40,41] These changes were accompanied by concomitant decreases in bone marrow HSC, MPP3/4, and pGM numbers (Figure S2). Since $Kmt2c^{\Delta/+}$ and $Kmt2c^{\Delta/\Delta}$ mice have more HSCs at steady state than wild-type mice, we calculated peripheral blood HSC numbers as the percentage of the total body HSC number. Even after normalizing for the larger HSC pool, *Kmt2c* deficiency led to more efficient HSC mobilization (Figure 1F). Thus, *Kmt2c* deletions enhance HSC and myeloid progenitor mobilization in response to G-CSF.

We next tested whether deleting *Kmt2c* in mature myeloid progenitors could similarly enhance HSC/myeloid progenitor mobilization and neutrophil production, or whether these phenotypes required deletion in immature progenitors. We treated $Cre^{-}$ control or *LyzM-Cre;* $Kmt2c^{f/f}$ mice with G-CSF for 4 days. *LyzM-Cre* deletes efficiently in neutrophils and monocytes/macrophages but not in a majority of HSCs.[42,43] Peripheral HSC, myeloid progenitor, and CFU numbers were similar in control and *LyzM-Cre;* $Kmt2c^{f/f}$ G-CSF-treated mice (Figure S3), indicating that *Kmt2c* primarily regulates mobilization through its activity in HSCs and MPPs.

We next tested whether *Kmt2c* deficiency enhances HSC mobilization following exposure to the CXCR4 antagonist plerixafor. We treated wild-type, $Kmt2c^{\Delta/+}$, and $Kmt2c^{\Delta/\Delta}$ mice with plerixafor (5 mg/kg)[44] and measured peripheral blood WBC and HSC numbers 2 h later. We did observe a significant increase in peripheral blood HSCs in $Kmt2c^{\Delta/\Delta}$ mice relative to both wild-type and $Kmt2c^{\Delta/+}$ mice (Figures S4A and S4B). However, the difference disappeared after normalization for the overall larger HSC population in $Kmt2c^{\Delta/\Delta}$ mice (Figure S4C), in contrast to the effects of *Kmt2c* deficiency on G-CSF-stimulated HSCs. Thus, *Kmt2c* deficiency enhances the mobilization of HSCs and myeloid progenitors in response to G-CSF but not plerixafor.

### *Kmt2c* deletions enhance HSCs and myeloid progenitor mobilization cells autonomously

We next tested whether *Kmt2c* deficiency enhances HSC and myeloid progenitor mobilization through cell-autonomous or non-cell-autonomous mechanisms. We generated mixed chimera recipient mice by transplanting 1 million wild-type, $Kmt2c^{\Delta/+}$, or $Kmt2c^{\Delta/\Delta}$ $CD45.2^{+}$ bone marrow cells into lethally irradiated recipient mice, along with 1 million wild-type $CD45.1^{+}$ competitor cells. We then treated the recipients with G-CSF, beginning at 6 weeks after transplantation. We measured $CD45.2^{+}$ and $CD45.1^{+}$ HSCs and myeloid progenitors in the bone marrow and peripheral blood of recipient mice after 4 days of vehicle or G-CSF treatment (Figure 2A). Donor peripheral blood chimerism was somewhat higher in recipients of *Kmt2c*-deficient bone marrow prior to G-CSF treatment (Figure 2B), consistent with our previous study.[31] However, $CD45.2^{+}$ and $CD45.1^{+}$ HSC and myeloid progenitor numbers were similar in the bone marrow of untreated mice for all *Kmt2c* genotypes, indicating that *Kmt2c*-deficient HSCs were not disproportionately

expanded relative to wild-type HSCs after transplant (Figures 2C and 2D). This finding is also consistent with our prior observations.[31] In contrast to the basal state, *Kmt2c*$^{\Delta/+}$ and *Kmt2c*$^{\Delta/\Delta}$ HSCs and myeloid progenitors displayed markedly enhanced mobilization, relative to CD45.1$^{+}$ wild-type progenitors, after 4 days of G-CSF treatment (Figures 2E and 2F). The data show that *Kmt2c* suppresses HSC and myeloid progenitor mobilization via cell-autonomous mechanisms.

## *Kmt2c* deletions promote rapid mobilization of HSCs and myeloid progenitors without enhancing proliferation rates

Our data raise the question of whether *Kmt2c* deficiency alters HSC proliferation in response to G-CSF or whether it simply accelerates the mobilization kinetics. Prior studies have shown that during the first 2 days of G-CSF exposure, HSCs proliferate in the bone marrow, and the HSC pool expands prior to mobilization.[1,3] However, more recent lineage-tracing studies have shown that HSCs mobilize without cycling.[45,46] We therefore tested whether *Kmt2c* deletions enhance HSC mobilization indirectly by amplifying proliferation in the bone marrow. We performed both 5′-bromo-2′-deoxyuridine (BrdU) incorporation assays and propidium iodide cell-cycle analyses to assess HSC, MPP, and myeloid progenitor (Lineage$^{-}$Sca1$^{-}$Kit$^{+}$) proliferation after 1 or 2 days of exposure to G-CSF. G-CSF did not significantly enhance bone marrow HSC proliferation at either time point (Figures 3A–3E), consistent with recent lineage tracing studies.[45,46] Furthermore, *Kmt2c* deletion did not alter HSC proliferation rates in either the absence or presence of G-CSF (Figures 3A–3E). MPP and myeloid progenitor proliferation rates were similarly unaffected by G-CSF and *Kmt2c* genotype (Figures 3B and 3E). Thus, *Kmt2c* deficiency does not enhance G-CSF-stimulated HSC and myeloid progenitor mobilization through changes in proliferation.

We next tested whether *Kmt2c* deficiency accelerates mobilization kinetics. In other words, do *Kmt2c*-deficient HSCs and myeloid progenitors transit to the peripheral blood more rapidly than wild-type HSCs and progenitors? We measured WBC, ANC, HSC, pGM, and GMP numbers in the peripheral blood after 2 days, rather than 4 days, of G-CSF treatment. At this early time point, wild-type HSCs, pGMs, and GMPs showed only modest degrees of mobilization (Figures 3F–3K). In contrast, peripheral WBC and ANC values were markedly elevated in G-CSF-treated *Kmt2c*$^{\Delta/\Delta}$ mice (Figures 3F and 3G), as were peripheral blood HSC, pGM, and GMP numbers (Figures 3H–3K). Thus, *Kmt2c* deletions accelerate HSC and myeloid progenitor mobilization without altering proliferation rates in these populations.

## *Kmt2c* deficiency suppresses inflammatory target gene expression and attenuates integrin expression in HSCs

We sought to identify *Kmt2c*-dependent mechanisms that restrict HSC mobilization and myeloid output following G-CSF exposure. We first tested whether *Kmt2c* deletions enhance G-CSF signal transduction. We treated wild-type and *Kmt2c*$^{\Delta/\Delta}$ HSC/MPPs, pGMs, and GMPs with G-CSF (10 ng/mL) for 30 min *ex vivo* and performed western blots to assess STAT3 phosphorylation. G-CSF induced similar levels of phosphorylation across all three populations, irrespective of *Kmt2c* genotype (Figure 4A). Phosphorylation of ribosomal protein S6 was similarly unaffected by *Kmt2c* genotype (Figure S5A). The data show that

*Kmt2c* deficiency does not enhance progenitor mobilization by amplifying G-CSF signal transduction.

We next performed CITE-seq to identify transcriptional changes that could enhance the mobilization of *Kmt2c*-deficient HSCs, MPPs, and myeloid progenitors. We isolated $Ter119^{-}B220^{-}CD3^{-}Kit^{+}$ progenitors after 2 days of G-CSF stimulation and performed CITE-seq with barcodes to various HSC/MPP and myeloid surface markers (CD201, CD150, CD48, SCA1, KIT, CD34, CD127, CD41, CD135, CD16/32, CD11B, and GR1). Biological replicate samples were marked with distinct surface barcodes for each of four conditions: wild type/vehicle, wild type/G-CSF, $Kmt2c^{\Delta/\Delta}$/vehicle, and $Kmt2c^{\Delta/\Delta}$/G-CSF (Table S1). This approach allowed us to map G-CSF-dependent changes in myelopoiesis across all $Kit^{+}$ myeloid progenitor populations. We clustered and visualized the data using partition-based graph abstraction (PAGA) and force-directed graphs, respectively.[47] A total of 19 clusters were assigned cell identities (e.g., HSC, myeloid, erythroid, megakaryocyte progenitors) based on the expression of select population-specific genes (Figures 4B and S5B).[48] In parallel, cells were assigned to specific populations–HSC, MPP3, MPP4, GMP, or myeloid ($CD11b^{+}$ $Gr1^{+}$)–based on surface marker phenotypes, as inferred from the feature barcodes (Figures 4B; and S5D). We could thus recapitulate myeloid differentiation in the context of the single-cell dataset.

The HSC population sat at the center of distinct myeloid and erythroid/megakaryocyte differentiation trajectories, irrespective of whether populations were defined by unsupervised clustering or surface marker phenotype (Figure 4B). Myeloid differentiation followed profoundly different trajectories in the presence and absence of G-CSF (Figure 4B). However, the trajectories were not appreciably different in wild-type or $Kmt2c^{\Delta/\Delta}$ progenitors, and they were highly reproducible among biological replicates (Figure S5C). We used diffusion pseudotime analysis to test whether *Kmt2c* deletion attenuates myeloid differentiation in the presence or absence of G-CSF.[47] We found that the degree of myeloid differentiation was generally higher in each phenotypically defined population in the presence of G-CSF, based on the pseudotime values for each cell, but *Kmt2c* deletion did not substantially attenuate differentiation (Figure 4C).

We used pseudobulk gene expression analysis to identify genes or pathways that distinguish G-CSF-treated wild-type and $Kmt2c^{\Delta/\Delta}$ HSCs, GMPs, and myeloid progenitors, with the goal of identifying pathways that could account for enhanced mobilization (Table S2). Gene set enrichment analysis (GSEA) showed highly significant downregulation of interferon-α target genes and other inflammatory pathways in G-CSF-treated $Kmt2c^{\Delta/\Delta}$ HSCs and other progenitors (Figures 4D and S6), consistent with our prior studies showing that *Kmt2c* potentiates inflammatory signaling in HSCs.[31] However, inactivating the interferon-α receptor gene *Ifnar1* did not hypersensitize HSC/MPPs to G-CSF, suggesting that *Kmt2c* deletion accelerates HSC mobilization via alternative mechanisms (Figures S7A–S7H).

We also observed strikingly lower expression of integrin and integrin signaling genes in $Kmt2c^{\Delta/\Delta}$ HSCs and GMPs, but not $CD11b^{+}/Gr1^{+}$ myeloid progenitors (Figures 4E and 4F). Affected integrins included several that are known to regulate HSC homing and that have been shown to restrict HSC mobilization, including *Itgal*, *Itga9*, *Itga4*, and *Itgb1*.[49–55] The

latter two integrin genes, *Itga4* (CD29) and *Itgb1* (CD49d), encode proteins that dimerize to form VLA-4, an adhesion molecule that has been targeted therapeutically to mobilize HSCs.[49–51] VLA-4 antagonists can greatly amplify G-CSF-induced mobilization, much like *Kmt2c* deficiency.[50,56] Flow cytometry confirmed that several of the integrins, including VLA-4 components, were downregulated in *Kmt2c*-deficient HSCs and myeloid progenitors (Figures 4G, 4H, S7I, and S7J). This quantitative reduction in integrin expression can at least partially account for the enhanced HSC and myeloid progenitor mobilization that was observed in $Kmt2c^{\Delta/\Delta}$ mice.

### *Kmt2c* deletion enhances granulocyte production from GMPs

We next tested whether *Kmt2c* modulates the expression of genes associated with myeloid differentiation in GMPs and $CD11b^{+}Gr1^{+}$ myeloid progenitors, as this could explain the exceptionally robust neutrophil output observed in $Kmt2c^{\Delta/\Delta}$ mice after G-CSF stimulation (Figures 1A and 1B). We used pseudobulk differential gene expression analysis to compare transcriptomes of wild-type and $Kmt2c^{\Delta/\Delta}$ GMPs. The comparison identified many genes that are associated with neutrophil identity and were more highly expressed in $Kmt2c^{\Delta/\Delta}$ as compared to wild-type GMPs (Figure 5A). GSEA confirmed the enrichment of neutrophil-associated genes in $Kmt2c^{\Delta/\Delta}$ GMPs and $Kmt2c^{\Delta/\Delta}$ $CD11b^{+}Gr1^{+}$ myeloid progenitors, suggesting that *Kmt2c* deficiency might bias GMPs toward granulocyte production (Figure 5B). GMP differentiation is regulated by antagonistic interactions of two transcription factors, IRF8, which promotes monocyte differentiation, and GFI1, which promotes granulocyte differentiation.[57,58] G-CSF suppressed *Irf8* expression and promoted *Gfi1* expression, but the changes were similar in both wild-type and $Kmt2c^{\Delta/\Delta}$ GMPs (Figure 5C). Likewise, other transcription factors associated with myeloid differentiation, such as *Spi1, Cepba*, *Cebpe*, and *Cebpb*,[57] were expressed at similar levels in wild-type and $Kmt2c^{\Delta/\Delta}$ GMPs (Figure S8). The data suggest that the *Kmt2c* loss accentuates granulocyte production at the expense of monocyte production by modulating targets of these transcription factors rather than the transcription factors themselves.

To test, functionally, whether *Kmt2c* loss enhances clonogenic potential and granulocyte differentiation from GMPs, we plated 300 GMPs in methylcellulose supplemented with myeloid cytokines (MethoCult M3434) and scored colonies 12–14 days later so that we could compare granulocyte and monocyte colony frequencies. We observed a modest but significant increase in $Kmt2c^{\Delta/\Delta}$ colony-forming unit colonies (CFU-Cs) relative to wild-type controls (Figure 5D). Furthermore, we detected a modest but significant depletion of colony-forming unit-monocyte colonies (CFU-Ms) and a corresponding but not statistically significant increase in colony-forming unit-granulocyte colonies (CFU-Gs) (Figure 5E). We next cultured wild-type and $Kmt2c^{\Delta/\Delta}$ GMPs for 5 days, with or without G-CSF supplementation (1 ng/mL), to test whether *Kmt2c* modulates granulocyte or monocyte output. Response to this very low dose of G-CSF was empirically established, and 1 ng/mL was chosen so that hypersensitivity to the cytokine could be resolved. Other myeloid-promoting cytokines (e.g., IL-3) were omitted from the culture media so that effects of G-CSF could be isolated. $Kmt2c^{\Delta/\Delta}$ GMPs gave rise to significantly more cells than wild-type GMPs, especially when cells were grown with G-CSF (Figure 5F). *In vitro* proliferation and cell death percentages were largely unaffected by either G-CSF stimulation or *Kmt2c*

deletion (Figures S9A and S9B), suggesting that the increase in cell numbers reflected reduced overall rates of differentiation in *Kmt2c*$^{\Delta/\Delta}$ GMPs.

As predicted by the CITE-seq studies, *Kmt2c* deficiency selectively amplified neutrophil production from G-CSF-stimulated GMPs. Cells cultured without G-CSF had immature progenitor morphologies, irrespective of *Kmt2c* genotype (Figure 5G). In contrast, cells cultured with G-CSF demonstrated monocyte or granulocyte differentiation, based on morphology (Figure 5G). *Kmt2c* deficiency led to substantially greater neutrophil production without significantly altering monocyte production (Figures 5H and 5I). *In vivo*, *Kmt2c* deficiency caused disproportionate neutrophil output following 4 days of G-CSF treatment, as evidenced by enhanced neutrophil/monocyte ratios (Figures 5J, S9C, and S9D). *Kmt2c* deficiency also exacerbated depletion of bone marrow dendritic cells (DCs) and macrophage numbers following G-CSF treatment (Figures 5K, 5L, S9E, and S9F). Thus, in addition to regulating HSC self-renewal and mobilization, *Kmt2c* restricts granulocyte production from GMPs, particularly in the context of G-CSF exposure.

## MLL3 inactivation enhances H3K27ac at regulatory elements associated with Hoxa family genes and neutrophil genes

Given that MLL3 promotes H3K4me1 and H3K27ac chromatin modifications, we sought to identify regulatory elements that could account for *Kmt2c*/MLL3-dependent changes in granulocyte production. We used new and previously described assay for transposase-accessible chromatin using sequencing (ATAC-seq) and H3K4me1 profiles[31] to identify enhancer elements (overlapping ATAC-seq and H3K4me1 peaks) in both HSC/MPPs and GMPs. We next measured H3K4me1 and H3K27ac levels at these elements by chromatin immunoprecipitation (ChIP)mentation.[59] Assays were performed on both wild-type and *Kmt2c*$^{\Delta/\Delta}$ backgrounds and in the presence and absence of G-CSF. Across all distal enhancer elements, G-CSF caused an increase in H3K4me1 levels (Figure 6A). The increase in H3K4me1 signal was similar in both wild-type and *Kmt2c*$^{\Delta/\Delta}$ HSC/MPPs, and it was paradoxically greatest in *Kmt2c*$^{\Delta/\Delta}$ GMPs (Figure 6A). H3K27ac levels were somewhat reduced across all enhancers in G-CSF-treated HSC/MPPs, irrespective of *Kmt2c* genotype, whereas H3K27ac levels were largely unaffected across all enhancers in G-CSF-treated GMPs (Figure 6B).

In contrast to the relatively modest effects of *Kmt2c* deletion on global enhancer H3K4me1 and H3K27ac levels, more substantive differences were observed near differentially expressed genes. Consistent with previous findings,[31] genes downregulated in *Kmt2c*$^{\Delta/\Delta}$ HSC/MPPs, such as *Il1r1*, had reduced enhancer-specific H3K4me1 and H3K27ac levels in the absence of G-CSF stimulation (Figures S10A and S10B). In contrast, genes that were expressed more highly in *Kmt2c*-deficient GMPs, relative to wild-type GMPs, demonstrated markedly higher levels of H3K27ac at promoter and enhancer elements, particularly after G-CSF treatment, that were not matched by corresponding changes in H3K4me1 (Figure 6C). Among the significantly elevated, *Kmt2c*-dependent H3K27ac peaks (as measured by diffbind) were several that mapped to *Hoxa5*, *Hoxa7*, and *Hoxa9* loci (Figure 6D). These genes are known to promote self-renewal when ectopically expressed in myeloid progenitors, and they are among the genes that were significantly more highly expressed

in *Kmt2c*$^{\Delta/\Delta}$ GMPs by CITE-seq (Table S2). H3K27ac levels were similarly elevated at enhancer and promoter elements that mapped near neutrophil-related genes, in this case defined by the Reactome neutrophil degranulation gene set that is more highly expressed in *Kmt2c*$^{\Delta/\Delta}$ GMPs relative to wild-type GMPs after G-CSF treatment (Figures 6E and 6F). Again, the increases in H3K27ac levels were not matched by corresponding changes in H3K4me1 levels. The data suggest that MLL3 dampens the expression of self-renewal and neutrophil differentiation genes indirectly and/or independently from its histone methyltransferase function.

### MLL3 methyltransferase activity is not required to restrict HSC repopulating activity, HSC mobilization, or granulocyte production in response to G-CSF

To test whether MLL3 requires its methyltransferase activity to regulate HSC mobilization and granulocyte production, we used CRISPR-Cas9 to generate a point mutation, Y4793A, that abrogates SET methyltransferase activity without attenuating protein expression (Figures 7A, 7B and S11).[37] Mice homozygous for the "SET-inactive" (SI) *Kmt2c* allele (*Kmt2c*$^{SI/SI}$) were viable and fertile, in contrast to mice with germline *Kmt2c*-null mutations.[31,35] This observation aligns with findings from an independently developed SI line with the same *Kmt2c* mutation.[37] *Kmt2c*$^{SI/SI}$ mice exhibited neither the increase in bone marrow HSC numbers nor the decrease in MPP3/4 numbers that typifies *Kmt2c*$^{\Delta/\Delta}$ mice (Figures 7C and 7D). As expected from prior studies,[31] *Kmt2c* mutations had no effect on basal GMP numbers (Figure 7E). Competitive transplantation assays showed that in contrast to *Kmt2c*$^{+/-}$ mice, HSCs from *Kmt2c*$^{SI/SI}$ mice have no repopulating advantage (Figure 7F). Thus, MLL3 does not require an active SET domain to promote HSC to MPP differentiation or to limit HSC repopulating activity.

To test whether the MLL3 SET domain modulates G-CSF sensitivity, we treated wild-type, *Kmt2c*$^{SI/SI}$, and *Kmt2c*$^{\Delta/\Delta}$ mice with G-CSF for 4 days and measured HSC mobilization and neutrophil production. Peripheral blood WBC, ANC, and CFU-C numbers were significantly elevated in G-CSF-treated *Kmt2c*$^{SI/SI}$ mice as compared to wild-type controls, but the changes were much smaller than were observed in *Kmt2c*$^{\Delta/\Delta}$ mice (Figures 7G–7I). *Kmt2c*$^{SI/SI}$ HSCs and MPPs did not mobilize to the peripheral blood or spleen at increased levels, relative to wild-type controls, again in contrast to *Kmt2c*$^{\Delta/\Delta}$ HSCs and MPPs (Figures 7J–7L). Thus, SET methyltransferase activity does not contribute to the restrictions that MLL3 imposes on HSC mobilization or granulocyte production following exposure to G-CSF.

## DISCUSSION

The data presented here show that *Kmt2c* deletions hypersensitize hematopoietic progenitors to G-CSF, with important implications for MDS/AML initiation. *Kmt2c*-deficient HSCs mobilize more efficiently than wild-type HSCs following G-CSF exposure. This mobilization phenotype coincides with the reduced expression of integrins that mediate HSC retention in the bone marrow, including *Itgb1* and *Itga4*, which encode subunits of VLA-4. While VLA-4 inhibition alone can cause low levels of HSC mobilization,[50,56] those effects were likely not observed in untreated *Kmt2c*$^{\Delta/\Delta}$ mice because expression levels were

only quantitatively reduced. G-CSF stimulation enabled more rapid and robust mobilization of *Kmt2c*$^{\Delta/\Delta}$ HSCs, akin to the synergy observed between VLA-4 antagonist and G-CSF in prior studies.[50,51,56] Other, currently unexplored mechanisms might also contribute to the enhanced mobilization of *Kmt2c*-deleted HSCs, but the parsimonious interpretation of our data and published literature is that quantitative reductions in integrin expression contribute to the mobilization phenotype.

The data highlight an important dichotomy in how *Kmt2c*/MLL3 regulates HSC cytokine responses. Inflammatory and interferon target genes were downregulated in *Kmt2c*-deficient HSCs, MPPs, and GMPs (Figure 4D), consistent with prior studies showing that *Kmt2c*/MLL3 mediates IL-1β target gene expression.[27,31] However, *Kmt2c* deletions simultaneously enhanced HSC, MPP, and GMP sensitivity to G-CSF. Both cytokine responses may contribute to MDS/AML initiation in the setting of a *KMT2C* mutation: reduced IL-1β and type I interferon sensitivity helps mitigate the loss of HSC self-renewal capacity after chemotherapy,[60–64] and G-CSF hypersensitivity helps amplify and mobilize the mutant HSC population.

In addition to enhancing progenitor mobilization, *Kmt2c* deficiency greatly amplifies granulocyte production from GMPs. The data point to at least two contributory mechanisms. First, *Kmt2c*$^{\Delta/\Delta}$ GMPs express self-renewal genes (*Hoxa5*, *Hoxa7*, *Hoxa9*, and *Prdm16*) at higher levels than wild-type GMPs (Figures 6D; Table S2). These genes have been implicated in leukemic transformation,[65,66] and their enhanced expression suggests that *Kmt2c*$^{\Delta/\Delta}$ GMPs retain greater self-renewal capacity than wild-type GMPs. CFU assays support this interpretation (Figure 5D). Second, *Kmt2c*$^{\Delta/\Delta}$ GMPs express genes associated with neutrophil identity at higher levels than wild-type GMPs, suggesting enhanced granulocyte bias. The imbalance does not reflect differences in the expression of myeloid transcription factors such as IRF8 or GFI1 (Figure 5C). Instead, self-renewal and neutrophil identity genes have higher levels of the activating H3K27ac mark at both proximal and distal regulatory elements. It is not clear why the loss of MLL3 leads to enhanced H3K27ac at these genes. One possibility is that MLL3 directly antagonizes other epigenetic regulators. Indeed, an antagonistic interaction between MLL1 and MLL3 has recently been described in AML.[67]

The epigenetic studies presented here suggested that MLL3 might restrict HSC repopulating activity, HSC mobilization, and granulopoiesis independently of its SET domain. We therefore developed a line of genetically altered mice to test this possibility. MLL3 SET inactivation had little to no effect on HSC repopulating activity, HSC mobilization after G-CSF treatment, or granulocyte production (Figure 7). Thus, several key functions of *Kmt2c*/MLL3 are mediated independently from the SET domain. This has therapeutic implications. In principle, one could transiently disrupt MLL3 activity to accelerate neutrophil recovery after chemotherapy while simultaneously negating any selective advantage that monosomy 7 clones derive from *KMT2C* haploinsufficiency (i.e., MLL3 function is transiently suppressed in all HSCs so monosomy 7 HSCs cannot gain a competitive advantage). Unfortunately, the SET domain does not offer a viable target for such a therapy because it does not appear to have a critical role in regulating HSC function.

Our findings ultimately highlight a potential complication that can arise from using G-CSF to promote hematopoietic recovery after chemotherapy and to mobilize HSCs for autologous stem cell transplants. If HSCs acquire a *KMT2C* mutation during early cycles of chemotherapy, as occurs with monosomy 7, the clone might be amplified by G-CSF exposure. Furthermore, *KMT2C*-mutant HSCs may disproportionately mobilize and become enriched within the stem cell collection product. G-CSF use could therefore enhance post-transplant therapy-related MDS/AML risk. In many cases, use of G-CSF is unavoidable, but it is noteworthy that plerixafor did not preferentially mobilize *Kmt2c*-deficient HSCs. Plerixafor may carry lower risks for therapy-related MDS/AML when used as a mobilizing agent than G-CSF. It remains an open question as to whether other leukemogenic mutations, such as *DNMT3A* or *TET2* mutations, similarly sensitize HSCs to G-CSF. Our data make a case for determining which MDS/AML mutations enhance G-CSF sensitivity and which do not.

### Limitations of the study

*KMT2C* is one of many genes that are deleted in the context of monosomy 7 in therapy-related MDS/AML. This study does not address how higher-order genetic interactions between these genes might influence G-CSF sensitivity, particularly in human progenitors. In addition, our understanding of the mechanisms that underlie G-CSF hypersensitivity of *Kmt2c*-deficient HSCs and GMPs likely remains incomplete. Finally, additional studies are needed to better understand how *KMT2C* deficiency predisposes to leukemic transformation (and the role of SET domain activity in this process), as the present study focused exclusively on non-malignant progenitors.

## STAR★METHODS

### RESOURCE AVAILABILTY

**Lead contact—**Further information and requests for reagents and resources should be directed to and will be fulfilled by the lead contact, Jeffrey Magee (mageej@wustl.edu).

**Materials availability—***Kmt2c*$^{f}$ mice are available from The Jackson Laboratory. The *Kmt2c*$^{SI}$ strain is available upon request. All other materials can be obtained from publicly available sources as noted below or in the Key Resources table.

### Data and code availability

- The datasets generated during this study are available at Gene Expression Omnibus under accession GSE243869.
- The paper does not report original code.
- Any additional information required to reanalyze the data reported in this paper is available from the lead contact upon request.

### EXPERIMENTAL MODEL AND STUDY PARTICIPANT DETAILS

**Mouse strains and treatments—***Kmt2c*$^{f}$ line was previously described[31] and all other mouse strains, with the exception of *Kmt2c*$^{SI}$ were obtained from the Jackson Laboratory.

*Kmt2c*$^{SI}$ mice were generated by the Washington University Genome Engineering and iPSC Center. Two guide RNAs (gRNA) were generated to target Cas9 nuclease to intronic sequence flanking the Y4793-encoding exon (the position of the mutated tyrosine is described based on amino acid annotation in GenBank: NP_001074852). Complexed gRNA/Cas9 were introduced into C57B6/J blastocysts by electroporation. A targeting cassette encoding the Y4793A missense mutation, the entire exon and flanking homology arms was delivered at the same time by recombinant Adeno-Associated Virus. Founder mice with successful incorporation of the targeting vector were identified and validated by next generation sequencing. Mice were subsequently genotyped by PCR by using primers targeting silent base substitutions (Figure S11) that were introduced into the coding sequence as part of the targeting cassette. The strain was maintained on a C57B6/J genetic background.

Male and female mice were used in similar numbers for all experiments, and all mice were evaluated at 8–12 weeks old, with the exception of transplant recipients. Mice were housed in a standard pathogen free barrier facility, and all procedures were performed according to an IACUC approved protocol at Washington University School of Medicine. G-CSF (Neupogen, Amgen) was diluted in sterile PBS containing 0.1% BSA and was given subcutaneously at a dose of 5 μg/day for 1, 2 or 4 consecutive days. Plerixafor (Adooq bioscience) was given subcutaneously at 5 mg/kg, 2 h before euthanizing the mice, as previously described.[44] For transplantation experiments, mice were gamma irradiated with two doses of 550 cGy spaced by 3 h. Cells were then injected to the retroorbital sinus.

## METHOD DETAILS

**Flow cytometry and colony formation assays—**Cells were isolated, stained, analyzed and transplanted as previously described,[76–78] using bone marrow, spleens or peripheral blood as source material. Peripheral blood was obtained from euthanized mice by cardiac puncture. Complete blood counts were obtained, and the remaining blood was subject to red blood cell lysis and staining as previously described.[39] Flow cytometry antibodies and surface marker phenotypes are defined in Table S3, and representative gating strategies are shown in Figures S1 and S8. Non-viable cells were excluded from analyses by 4′,6-diamidino-2-phenylindone (DAPI) staining (1 μg/mL except as indicated below). Flow cytometry was performed on a BD FACSAria Fusion flow cytometer (BD Biosciences). For analysis of integrin expression, mean fluorescent intensity values were calculated in FlowJo. Colony formation assays were performed by culturing the indicated cells in Methocult M3434 media (Stem Cell Technologies). Colony morphologies were scored 12–14 days later.

**CITE-seq library construction, sequencing and analysis—**Adult bone marrow cells were isolated after two days of vehicle or G-CSF treatment. Cells were c-Kit selected, and 2 million cells were then stained with tagged Total-Seq B antibodies (Biolegend) to CD150, CD48, CD135, CD34, CD201, CD117 (2B8 clone), Sca1, CD16/32, CD127, CD41, Gr1, and CD11b. We isolated Ter119$^{-}$B220$^{-}$CD3$^{-}$Kit$^{+}$ cells (LK) by flow cytometry and generated libraries with 10x Genomics Chromium Next GEM Single Cell 3′ v3.1, Chromium Single Cell 3′ Feature Barcode Library, Dual Index NT Set A, and Dual Index

TT Set A kits according to the manufacturer's instructions. Libraries were sequenced on an Illumina Novaseq S4. The Cell Ranger v.6.0.1 pipeline (10x Genomics) was used to process data. Digital gene expression (DGE) files were then filtered and normalized as previously described.[76] Expression of antibody directed tags was calculated for each cell in Seurat.[68,69] Population identities were assigned to cells based on antibody directed tags as previously described.[77,79] Clustering, force directed graphs and pseudotime analyses were performed with Scanpy and PAGA.[47] Differential expression analyses were performed by combining cells from biological replicates ($n = 2$ per condition/genotype) and pseudoreplicates ($n = 2$ per replicate) to generate pseudobulk samples for each cluster using Presto.[72] Pseudobulk samples were compared using DESeq2[70] and GSEA.[71]

**Cell cycle, BrdU incorporation and annexin V assays—**Cell cycle, 5′-bromo-2′-deoxyuridine (BrdU) and Annexin V assays were performed as previously described.[31,76] For BrdU incorporation assays, mice were injected with BrdU (150 mg/kg body weight) 24 h before cell collection and then placed on BrdU drinking water (1 mg/mL). The assay was carried out using BrdU flow cytometry kits per manufacturer instructions (BD Pharmigen). For propidium iodide cell cycle stains, cells were sorted into 70% ethanol and incubated at 4°C overnight. Cells were then washed twice with PBS to remove fixative and re-suspended in 0.3 mL of FxCycle PI/RNase staining solution (Invitrogen) for analysis.

**Primary cell cultures—**GMPs (1000 cells per assay) were isolated by flow cytometry and cultured in StemSpan SFEM II (Stem Cell Technologies) supplemented with SCF (100 ng/mL) for 5 days, with or without G-CSF (1 ng/mL). Cell counts were obtained using a hemacytometer. For morphology assays, $Gr1^+CD11b^+$ cells were sorted, cytospun and Wright-Giemsa stained.

**Western blots—**For analysis of STAT3 and S6 phosphorylation, 30,000 cells were sorted into PBS with 0.1% BSA. Cells were then resuspended in RPMI with 2% FBS, with or without G-CSF (10 ng/mL) as indicated. Cells were incubated at 37°C for 30 min, washed and transferred to 10% Trichloracetic acid. The precipitates were pelleted, washed with acetone and solubilized for Western blotting as previously described.[78] For analysis of MLL3 expression, 3 million mouse embryonic fibroblasts of the indicated genotypes were washed with cold PBS. Cells were resuspended in cold buffer (10mM NaCl, 10mM Tris pH7.5, 3mM MgCl2 with protease inhibitor) and incubated on ice for 5 min. Nuclei were pelleted and resuspended in modified RIPA buffer (0.1% IGEPAL, 0.1% sodium deoxycholate, 150mM NaCl, 50mM Tris pH7.5, 1 U/μL Benzonase and 1mM MgCl2 with protease inhibitor). Cells were incubated on ice for 20 min and debris was removed by centrifugation. Antibodies are listed in Table S3. The MLL3 antibody was provided by Kai Ge and has been described previously.[80]

**ChIPmentation and ATAC-seq—**75,000 $Lin^-Kit^+Sca1^+$ cells or 92,000 GMPs were double sorted into PBS +0.1% BSA. ChIPmentation was performed as previously described.[59,76] Sonication was performed with a Covaris E220 using empirically defined setting (Peak incident power 105, duty factor 2%, cycles per burst 200, duration 840s). After sonication, each sample was equally distributed for overnight incubation with either

H3K4me1 or H3K27ac antibodies from Diagenode. After library amplification, fragments were size selected with SPRI beads with ratios of 0.65x and 0.9x for right- and left-sided selection. Sequencing was performed on a NovaSeq X Plus. Reads were mapped to mm10, peaks were called with MACS2[81] and compared with diffbind, to identify peaks with significant differences in histone modifications. Tracks were visualized in the WashU Epigenome Browser[82] using pipelines that we have described previously.[31]

A list HSC/MPP distal enhancers was previously defined[31,76] and was evaluated in this study for changes in H3K4me1 and H3K27ac as indicated. A list of GMP distal enhancers was defined by performing ATAC-seq on 50,000 GMPs using previously described methods[73–76] and identifying peaks that overlap with H3K4me1 peaks in wildtype GMPs. Proximal promoter elements were defined as regions 2 kb upstream of the transcriptional start site of each gene.

### QUANTIFICATION AND STATISTICAL ANALYSIS

Group sizes are indicated in the figure legends. Groups were compared with one way ANOVA and Holm-Sidak posthoc test to correct for multiple comparisons. CITE-seq analyses are described above. Survival data were compared with the log-rank test.

## Supplementary Material

Refer to Web version on PubMed Central for supplementary material.

## ACKNOWLEDGMENTS

We thank J. Michael White in the Department of Pathology Transgenic Mouse core and Xiaoxia Cui in the Genome Engineering and iPSC center at Washington University for assistance in generating the *Kmt2c*$^{SI}$ mouse strain. We thank Dr. Kai Ge at the NIH for the MLL3 antibody. This work was supported by grants to J.A.M. from the National Heart, Lung, and Blood Institute (R01 HL152180 and R01 HL136504), Alex's Lemonade Stand Foundation ("A" Award), the Edward P. Evans Foundation, the Alvin J. Siteman Cancer Center Investment Program (supported by the Foundation for Barnes-Jewish Hospital and NCI Cancer Center Support Grant P30 CA091842), and the Children's Discovery Institute of Washington University and St. Louis Children's Hospital. J.A.M. is a Scholar of the Leukemia and Lymphoma Society.

## REFERENCES

1. Morrison SJ, Wright DE, and Weissman IL (1997). Cyclophosphamide/granulocyte colony-stimulating factor induces hematopoietic stem cells to proliferate prior to mobilization. Proc. Natl. Acad. Sci. USA 94, 1908–1913. [PubMed: 9050878]
2. McLemore ML, Grewal S, Liu F, Archambault A, Poursine-Laurent J, Haug J, and Link DC (2001). STAT-3 activation is required for normal G-CSF-dependent proliferation and granulocytic differentiation. Immunity 14, 193–204. 10.1016/s1074-7613(01)00101-7. [PubMed: 11239451]
3. Schuettpelz LG, Borgerding JN, Christopher MJ, Gopalan PK, Romine MP, Herman AC, Woloszynek JR, Greenbaum AM, and Link DC (2014). G-CSF regulates hematopoietic stem cell activity, in part, through activation of Toll-like receptor signaling. Leukemia 28, 1851–1860. 10.1038/leu.2014.68. [PubMed: 24518205]
4. Greenbaum AM, and Link DC (2011). Mechanisms of G-CSF-mediated hematopoietic stem and progenitor mobilization. Leukemia 25, 211–217. 10.1038/leu.2010.248. [PubMed: 21079612]
5. Hareng L, and Hartung T (2002). Induction and regulation of endogenous granulocyte colony-stimulating factor formation. Biol. Chem. 383, 1501–1517. 10.1515/BC.2002.172. [PubMed: 12452428]

6. Boettcher S, Gerosa RC, Radpour R, Bauer J, Ampenberger F, Heikenwalder M, Kopf M, and Manz MG (2014). Endothelial cells translate pathogen signals into G-CSF-driven emergency granulopoiesis. Blood 124, 1393–1403. 10.1182/blood-2014-04-570762. [PubMed: 24990886]

7. Burberry A, Zeng MY, Ding L, Wicks I, Inohara N, Morrison SJ, and Nunez G (2014). Infection mobilizes hematopoietic stem cells through cooperative NOD-like receptor and Toll-like receptor signaling. Cell Host Microbe 15, 779–791. 10.1016/j.chom.2014.05.004. [PubMed: 24882704]

8. Dale DC, Bonilla MA, Davis MW, Nakanishi AM, Hammond WP, Kurtzberg J, Wang W, Jakubowski A, Winton E, Lalezari P, et al. (1993). A randomized controlled phase III trial of recombinant human granulocyte colony-stimulating factor (filgrastim) for treatment of severe chronic neutropenia. Blood 81, 2496–2502. [PubMed: 8490166]

9. Hopman RK, and DiPersio JF (2014). Advances in stem cell mobilization. Blood Rev. 28, 31–40. 10.1016/j.blre.2014.01.001. [PubMed: 24476957]

10. Renwick W, Pettengell R, and Green M (2009). Use of filgrastim and pegfilgrastim to support delivery of chemotherapy: twenty years of clinical experience. BioDrugs 23, 175–186. 10.2165/00063030-200923030-00004. [PubMed: 19627169]

11. Germeshausen M, Ballmaier M, and Welte K (2007). Incidence of CSF3R mutations in severe congenital neutropenia and relevance for leukemogenesis: Results of a long-term survey. Blood 109, 93–99. 10.1182/blood-2006-02-004275. [PubMed: 16985178]

12. Link DC (2019). Mechanisms of leukemic transformation in congenital neutropenia. Curr. Opin. Hematol. 26, 34–40. 10.1097/MOH.0000000000000479. [PubMed: 30431463]

13. McNerney ME, Godley LA, and Le Beau MM (2017). Therapy-related myeloid neoplasms: when genetics and environment collide. Nat. Rev. Cancer 17, 513–527. 10.1038/nrc.2017.60. [PubMed: 28835720]

14. Hsu JI, Dayaram T, Tovy A, De Braekeleer E, Jeong M, Wang F, Zhang J, Heffernan TP, Gera S, Kovacs JJ, et al. (2018). PPM1D Mutations Drive Clonal Hematopoiesis in Response to Cytotoxic Chemotherapy. Cell Stem Cell 23, 700–713.e6. 10.1016/j.stem.2018.10.004. [PubMed: 30388424]

15. Coombs CC, Zehir A, Devlin SM, Kishtagari A, Syed A, Jonsson P, Hyman DM, Solit DB, Robson ME, Baselga J, et al. (2017). Therapy-Related Clonal Hematopoiesis in Patients with Non-hematologic Cancers Is Common and Associated with Adverse Clinical Outcomes. Cell Stem Cell 21, 374–382.e4. 10.1016/j.stem.2017.07.010. [PubMed: 28803919]

16. Kahn JD, Miller PG, Silver AJ, Sellar RS, Bhatt S, Gibson C, McConkey M, Adams D, Mar B, Mertins P, et al. (2018). PPM1D-truncating mutations confer resistance to chemotherapy and sensitivity to PPM1D inhibition in hematopoietic cells. Blood 132, 1095–1105. 10.1182/blood-2018-05-850339. [PubMed: 29954749]

17. Wong TN, Miller CA, Jotte MRM, Bagegni N, Baty JD, Schmidt AP, Cashen AF, Duncavage EJ, Helton NM, Fiala M, et al. (2018). Cellular stressors contribute to the expansion of hematopoietic clones of varying leukemic potential. Nat. Commun. 9, 455. 10.1038/s41467-018-02858-0. [PubMed: 29386642]

18. Will B, Zhou L, Vogler TO, Ben-Neriah S, Schinke C, Tamari R, Yu Y, Bhagat TD, Bhattacharyya S, Barreyro L, et al. (2012). Stem and progenitor cells in myelodysplastic syndromes show aberrant stage-specific expansion and harbor genetic and epigenetic alterations. Blood 120, 2076–2086. 10.1182/blood-2011-12-399683. [PubMed: 22753872]

19. Inaba T, Honda H, and Matsui H (2018). The enigma of monosomy 7. Blood 131, 2891–2898. 10.1182/blood-2017-12-822262. [PubMed: 29615405]

20. Jerez A, Sugimoto Y, Makishima H, Verma A, Jankowska AM, Przychodzen B, Visconte V, Tiu RV, O'Keefe CL, Mohamedali AM, et al. (2012). Loss of heterozygosity in 7q myeloid disorders: clinical associations and genomic pathogenesis. Blood 119, 6109–6117. 10.1182/blood-2011-12-397620. [PubMed: 22553315]

21. Sloand EM, Yong AS, Ramkissoon S, Solomou E, Bruno TC, Kim S, Fuhrer M, Kajigaya S, Barrett AJ, and Young NS (2006). Granulocyte colony-stimulating factor preferentially stimulates proliferation of monosomy 7 cells bearing the isoform IV receptor. Proc. Natl. Acad. Sci. USA 103, 14483–14488. 10.1073/pnas.0605245103. [PubMed: 16980411]

22. Hirsch B, Oseth L, Cain M, Trader E, Pulkrabek S, Lindgren B, Luo X, Clay M, Miller J, Confer D, et al. (2011). Effects of granulocyte-colony stimulating factor on chromosome aneuploidy

and replication asynchrony in healthy peripheral blood stem cell donors. Blood 118, 2602–2608. 10.1182/blood-2011-04-348508. [PubMed: 21719598]

23. Nagasawa M, Tomizawa D, Tsuji Y, Kajiwara M, Morio T, Nonoyama S, Asada M, and Mizutani S (2004). Pancytopenia presenting with monosomy 7 which disappeared after immunosuppressive therapy. Leuk. Res. 28, 315–319. 10.1016/s0145-2126(03)00263-7. [PubMed: 14687628]
24. Hosono N, Makishima H, Jerez A, Yoshida K, Przychodzen B, McMahon S, Shiraishi Y, Chiba K, Tanaka H, Miyano S, et al. (2014). Recurrent genetic defects on chromosome 7q in myeloid neoplasms. Leukemia 28, 1348–1351. 10.1038/leu.2014.25. [PubMed: 24429498]
25. Zhou L, Opalinska J, Sohal D, Yu Y, Mo Y, Bhagat T, Abdel-Wahab O, Fazzari M, Figueroa M, Alencar C, et al. (2011). Aberrant epigenetic and genetic marks are seen in myelodysplastic leukocytes and reveal Dock4 as a candidate pathogenic gene on chromosome 7q. J. Biol. Chem. 286, 25211–25223. 10.1074/jbc.M111.235028. [PubMed: 21532034]
26. Poetsch AR, Lipka DB, Witte T, Claus R, Nollke P, Zucknick M, Olk-Batz C, Fluhr S, Dworzak M, De Moerloose B, et al. (2014). RASA4 undergoes DNA hypermethylation in resistant juvenile myelomonocytic leukemia. Epigenetics 9, 1252–1260. 10.4161/epi.29941. [PubMed: 25147919]
27. Chen C, Liu Y, Rappaport AR, Kitzing T, Schultz N, Zhao Z, Shroff AS, Dickins RA, Vakoc CR, Bradner JE, et al. (2014). MLL3 is a haploinsufficient 7q tumor suppressor in acute myeloid leukemia. Cancer Cell 25, 652–665. 10.1016/j.ccr.2014.03.016. [PubMed: 24794707]
28. An N, Khan S, Imgruet MK, Gurbuxani SK, Konecki SN, Burgess MR, and McNerney ME (2018). Gene dosage effect of CUX1 in a murine model disrupts HSC homeostasis and controls the severity and mortality of MDS. Blood 131, 2682–2697. 10.1182/blood-2017-10-810028. [PubMed: 29592892]
29. Shih AH, Jiang Y, Meydan C, Shank K, Pandey S, Barreyro L, Antony-Debre I, Viale A, Socci N, Sun Y, et al. (2015). Mutational cooperativity linked to combinatorial epigenetic gain of function in acute myeloid leukemia. Cancer Cell 27, 502–515. 10.1016/j.ccell.2015.03.009. [PubMed: 25873173]
30. Wong JC, Weinfurtner KM, Alzamora Mdel P, Kogan SC, Burgess MR, Zhang Y, Nakitandwe J, Ma J, Cheng J, Chen SC, et al. (2015). Functional evidence implicating chromosome 7q22 haploinsufficiency in myelodysplastic syndrome pathogenesis. Elife 4, e07839. 10.7554/eLife.07839. [PubMed: 26193121]
31. Chen R, Okeyo-Owuor T, Patel RM, Casey EB, Cluster AS, Yang W, and Magee JA (2021). Kmt2c mutations enhance HSC self-renewal capacity and convey a selective advantage after chemotherapy. Cell Rep. 34, 108751. 10.1016/j.celrep.2021.108751. [PubMed: 33596429]
32. Herz HM, Mohan M, Garruss AS, Liang K, Takahashi YH, Mickey K, Voets O, Verrijzer CP, and Shilatifard A (2012). Enhancer-associated H3K4 monomethylation by Trithorax-related, the Drosophila homolog of mammalian Mll3/Mll4. Genes Dev. 26, 2604–2620. 10.1101/gad.201327.112. [PubMed: 23166019]
33. Hu D, Gao X, Morgan MA, Herz HM, Smith ER, and Shilatifard A (2013). The MLL3/MLL4 branches of the COMPASS family function as major histone H3K4 monomethylases at enhancers. Mol. Cell Biol. 33, 4745–4754. 10.1128/MCB.01181-13. [PubMed: 24081332]
34. Sze CC, and Shilatifard A (2016). MLL3/MLL4/COMPASS Family on Epigenetic Regulation of Enhancer Function and Cancer. Cold Spring Harb. Perspect. Med. 6, a026427. 10.1101/cshperspect.a026427. [PubMed: 27638352]
35. Dorighi KM, Swigut T, Henriques T, Bhanu NV, Scruggs BS, Nady N, Still CD 2nd, Garcia BA, Adelman K, and Wysocka J. (2017). Mll3 and Mll4 Facilitate Enhancer RNA Synthesis and Transcription from Promoters Independently of H3K4 Monomethylation. Mol. Cell 66, 568–576.e4. 10.1016/j.molcel.2017.04.018. [PubMed: 28483418]
36. Rickels R, Herz HM, Sze CC, Cao K, Morgan MA, Collings CK, Gause M, Takahashi YH, Wang L, Rendleman EJ, et al. (2017). Histone H3K4 monomethylation catalyzed by Trr and mammalian COMPASS-like proteins at enhancers is dispensable for development and viability. Nat. Genet. 49, 1647–1653. 10.1038/ng.3965. [PubMed: 28967912]
37. Xie G, Lee JE, Senft AD, Park YK, Jang Y, Chakraborty S, Thompson JJ, McKernan K, Liu C, Macfarlan TS, et al. (2023). MLL3/MLL4 methyltransferase activities control early embryonic development and embryonic stem cell differentiation in a lineage-selective manner. Nat. Genet. 55, 693–705. 10.1038/s41588-023-01356-4. [PubMed: 37012455]

38. Lai B, Lee JE, Jang Y, Wang L, Peng W, and Ge K (2017). MLL3/MLL4 are required for CBP/p300 binding on enhancers and super-enhancer formation in brown adipogenesis. Nucleic Acids Res. 45, 6388–6403. 10.1093/nar/gkx234. [PubMed: 28398509]
39. Porter SN, Cluster AS, Signer RA, Voigtmann J, Monlish DA, Schuettpelz LG, and Magee JA (2016). Pten Cell Autonomously Modulates the Hematopoietic Stem Cell Response to Inflammatory Cytokines. Stem Cell Rep. 6, 806–814. 10.1016/j.stemcr.2016.04.008.
40. Pietras EM, Reynaud D, Kang YA, Carlin D, Calero-Nieto FJ, Leavitt AD, Stuart JM, Gottgens B, and Passegue E (2015). Functionally Distinct Subsets of Lineage-Biased Multipotent Progenitors Control Blood Production in Normal and Regenerative Conditions. Cell Stem Cell 17, 35–46. 10.1016/j.stem.2015.05.003. [PubMed: 26095048]
41. Pronk CJ, Rossi DJ, Mansson R, Attema JL, Norddahl GL, Chan CK, Sigvardsson M, Weissman IL, and Bryder D (2007). Elucidation of the phenotypic, functional, and molecular topography of a myeloerythroid progenitor cell hierarchy. Cell Stem Cell 1, 428–442. 10.1016/j.stem.2007.07.005. [PubMed: 18371379]
42. Clausen BE, Burkhardt C, Reith W, Renkawitz R, and Forster I (1999). Conditional gene targeting in macrophages and granulocytes using LysMcre mice. Transgenic Res. 8, 265–277. [PubMed: 10621974]
43. Abram CL, Roberge GL, Hu Y, and Lowell CA (2014). Comparative analysis of the efficiency and specificity of myeloid-Cre deleting strains using ROSA-EYFP reporter mice. J. Immunol. Methods 408, 89–100. 10.1016/j.jim.2014.05.009. [PubMed: 24857755]
44. Devine SM, Vij R, Rettig M, Todt L, McGlauchlen K, Fisher N, Devine H, Link DC, Calandra G, Bridger G, et al. (2008). Rapid mobilization of functional donor hematopoietic cells without G-CSF using AMD3100, an antagonist of the CXCR4/SDF-1 interaction. Blood 112, 990–998. 10.1182/blood-2007-12-130179. [PubMed: 18426988]
45. Bernitz JM, Daniel MG, Fstkchyan YS, and Moore K (2017). Granulocyte colony-stimulating factor mobilizes dormant hematopoietic stem cells without proliferation in mice. Blood 129, 1901–1912. 10.1182/blood-2016-11-752923. [PubMed: 28179275]
46. Munz CM, Dressel N, Chen M, Grinenko T, Roers A, and Gerbaulet A (2023). Regeneration after blood loss and acute inflammation proceeds without contribution of primitive HSCs. Blood 141, 2483–2492. 10.1182/blood.2022018996. [PubMed: 36787502]
47. Wolf FA, Hamey FK, Plass M, Solana J, Dahlin JS, Gottgens B, Rajewsky N, Simon L, and Theis FJ (2019). PAGA: graph abstraction reconciles clustering with trajectory inference through a topology preserving map of single cells. Genome Biol. 20, 59. 10.1186/s13059-019-1663-x. [PubMed: 30890159]
48. Paul F, Arkin Y, Giladi A, Jaitin DA, Kenigsberg E, Keren-Shaul H, Winter D, Lara-Astiaso D, Gury M, Weiner A, et al. (2015). Transcriptional Heterogeneity and Lineage Commitment in Myeloid Progenitors. Cell 163, 1663–1677. 10.1016/j.cell.2015.11.013. [PubMed: 26627738]
49. Karpova D, Rettig MP, Ritchey J, Cancilla D, Christ S, Gehrs L, Chendamarai E, Evbuomwan MO, Holt M, Zhang J, et al. (2019). Targeting VLA4 integrin and CXCR2 mobilizes serially repopulating hematopoietic stem cells. J. Clin. Invest. 129, 2745–2759. 10.1172/JCI124738. [PubMed: 31085833]
50. Ramirez P, Rettig MP, Uy GL, Deych E, Holt MS, Ritchey JK, and DiPersio JF (2009). BIO5192, a small molecule inhibitor of VLA-4, mobilizes hematopoietic stem and progenitor cells. Blood 114, 1340–1343. 10.1182/blood-2008-10-184721. [PubMed: 19571319]
51. Rettig MP, Ansstas G, and DiPersio JF (2012). Mobilization of hematopoietic stem and progenitor cells using inhibitors of CXCR4 and VLA-4. Leukemia 26, 34–53. 10.1038/leu.2011.197. [PubMed: 21886173]
52. Velders GA, Pruijt JF, Verzaal P, van Os R, van Kooyk Y, Figdor CG, de Kruijf EJ, Willemze R, and Fibbe WE (2002). Enhancement of G-CSF-induced stem cell mobilization by antibodies against the beta 2 integrins LFA-1 and Mac-1. Blood 100, 327–333. 10.1182/blood.v100.1.327. [PubMed: 12070044]
53. Schreiber TD, Steinl C, Essl M, Abele H, Geiger K, Muller CA, Aicher WK, and Klein G (2009). The integrin alpha9beta1 on hematopoietic stem and progenitor cells: involvement in cell adhesion, proliferation and differentiation. Haematologica 94, 1493–1501. 10.3324/haematol.2009.006072. [PubMed: 19608669]

54. Grassinger J, Haylock DN, Storan MJ, Haines GO, Williams B, Whitty GA, Vinson AR, Be CL, Li S, Sorensen ES, et al. (2009). Thrombin-cleaved osteopontin regulates hemopoietic stem and progenitor cell functions through interactions with alpha9beta1 and alpha4beta1 integrins. Blood 114, 49–59. 10.1182/blood-2009-01-197988. [PubMed: 19417209]
55. Qian H, Tryggvason K, Jacobsen SE, and Ekblom M (2006). Contribution of alpha6 integrins to hematopoietic stem and progenitor cell homing to bone marrow and collaboration with alpha4 integrins. Blood 107, 3503–3510. 10.1182/blood-2005-10-3932. [PubMed: 16439681]
56. Craddock CF, Nakamoto B, Andrews RG, Priestley GV, and Papayannopoulou T (1997). Antibodies to VLA4 integrin mobilize long-term repopulating cells and augment cytokine-induced mobilization in primates and mice. Blood 90, 4779–4788. [PubMed: 9389694]
57. Rosenbauer F, and Tenen DG (2007). Transcription factors in myeloid development: balancing differentiation with transformation. Nat. Rev. Immunol. 7, 105–117. 10.1038/nri2024. [PubMed: 17259967]
58. Olsson A, Venkatasubramanian M, Chaudhri VK, Aronow BJ, Salomonis N, Singh H, and Grimes HL (2016). Single-cell analysis of mixed-lineage states leading to a binary cell fate choice. Nature 537, 698–702. 10.1038/nature19348. [PubMed: 27580035]
59. Schmidl C, Rendeiro AF, Sheffield NC, and Bock C (2015). ChIP-mentation: fast, robust, low-input ChIP-seq for histones and transcription factors. Nat. Methods 12, 963–965. 10.1038/nmeth.3542. [PubMed: 26280331]
60. Chavez JS, Rabe JL, Loeffler D, Higa KC, Hernandez G, Mills TS, Ahmed N, Gessner RL, Ke Z, Idler BM, et al. (2021). PU.1 enforces quiescence and limits hematopoietic stem cell expansion during inflammatory stress. J. Exp. Med. 218, e20201169. 10.1084/jem.20201169. [PubMed: 33857288]
61. Pietras EM, Mirantes-Barbeito C, Fong S, Loeffler D, Kovtonyuk LV, Zhang S, Lakshminarasimhan R, Chin CP, Techner JM, Will B, et al. (2016). Chronic interleukin-1 exposure drives haematopoietic stem cells towards precocious myeloid differentiation at the expense of self-renewal. Nat. Cell Biol. 18, 607–618. 10.1038/ncb3346. [PubMed: 27111842]
62. Kovtonyuk LV, Caiado F, Garcia-Martin S, Manz EM, Helbling P, Takizawa H, Boettcher S, Al-Shahrour F, Nombela-Arrieta C, Slack E, and Manz MG (2022). IL-1 mediates microbiome-induced inflammaging of hematopoietic stem cells in mice. Blood 139, 44–58. 10.1182/blood.2021011570. [PubMed: 34525198]
63. Caiado F, Kovtonyuk LV, Gonullu NG, Fullin J, Boettcher S, and Manz MG (2023). Aging drives Tet2+/− clonal hematopoiesis via IL-1 signaling. Blood 141, 886–903. 10.1182/blood.2022016835. [PubMed: 36379023]
64. Walter D, Lier A, Geiselhart A, Thalheimer FB, Huntscha S, Sobotta MC, Moehrle B, Brocks D, Bayindir I, Kaschutnig P, et al. (2015). Exit from dormancy provokes DNA-damage-induced attrition in haematopoietic stem cells. Nature 520, 549–552. 10.1038/nature14131. [PubMed: 25707806]
65. Hu T, Morita K, Hill MC, Jiang Y, Kitano A, Saito Y, Wang F, Mao X, Hoegenauer KA, Morishita K, et al. (2019). PRDM16s transforms megakaryocyte-erythroid progenitors into myeloid leukemia-initiating cells. Blood 134, 614–625. 10.1182/blood.2018888255. [PubMed: 31270104]
66. Bach C, Buhl S, Mueller D, Garcia-Cuellar MP, Maethner E, and Slany RK (2010). Leukemogenic transformation by HOXA cluster genes. Blood 115, 2910–2918. 10.1182/blood-2009-04-216606. [PubMed: 20130239]
67. Soto-Feliciano YM, Sanchez-Rivera FJ, Perner F, Barrows DW, Kastenhuber ER, Ho YJ, Carroll T, Xiong Y, Anand D, Soshnev AA, et al. (2023). A Molecular Switch between Mammalian MLL Complexes Dictates Response to Menin-MLL Inhibition. Cancer Discov. 13, 146–169. 10.1158/2159-8290.CD-22-0416. [PubMed: 36264143]
68. Butler A, Hoffman P, Smibert P, Papalexi E, and Satija R (2018). Integrating single-cell transcriptomic data across different conditions, technologies, and species. Nat. Biotechnol. 36, 411–420. 10.1038/nbt.4096. [PubMed: 29608179]
69. Stuart T, Srivastava A, Madad S, Lareau CA, and Satija R (2021). Single-cell chromatin state analysis with Signac. Nat. Methods 18, 1333–1341. 10.1038/s41592-021-01282-5. [PubMed: 34725479]

70. Love MI, Huber W, and Anders S (2014). Moderated estimation of fold change and dispersion for RNA-seq data with DESeq2. Genome Biol. 15, 550. 10.1186/s13059-014-0550-8. [PubMed: 25516281]
71. Subramanian A, Tamayo P, Mootha VK, Mukherjee S, Ebert BL, Gillette MA, Paulovich A, Pomeroy SL, Golub TR, Lander ES, and Mesirov JP (2005). Gene set enrichment analysis: a knowledge--based approach for interpreting genome-wide expression profiles. Proc. Natl. Acad. Sci. USA 102, 15545–15550. 10.1073/pnas.0506580102. [PubMed: 16199517]
72. Korsunsky I, Nathan A, Millard N, and Raychaudhuri S (2019). Presto scales Wilcoxon and auROC analyses to millions of observations. Preprint at bioRxiv. 10.1101/653253.
73. Corces MR, Trevino AE, Hamilton EG, Greenside PG, Sinnott-Armstrong NA, Vesuna S, Satpathy AT, Rubin AJ, Montine KS, Wu B, et al. (2017). An improved ATAC-seq protocol reduces background and enables interrogation of frozen tissues. Nat. Methods 14, 959–962. 10.1038/nmeth.4396. [PubMed: 28846090]
74. Li Q, Brown JB, Huang H, and Bickel PJ (2011). Measuring reproducibility of high-throughput experiments. Ann. Appl. Stat. 5, 1752–1779.
75. Roadmap Epigenomics Consortium; Kundaje A, Meuleman W, Ernst J, Bilenky M, Yen A, Heravi-Moussavi A, Kheradpour P, Zhang Z, Wang J, et al. (2015). Integrative analysis of 111 reference human epigenomes. Nature 518, 317–330. 10.1038/nature14248. [PubMed: 25693563]
76. Li Y, Kong W, Yang W, Patel RM, Casey EB, Okeyo-Owuor T, White JM, Porter SN, Morris SA, and Magee JA (2020). Single-Cell Analysis of Neonatal HSC Ontogeny Reveals Gradual and Uncoordinated Transcriptional Reprogramming that Begins before Birth. Cell Stem Cell 27, 732–747.e7. 10.1016/j.stem.2020.08.001. [PubMed: 32822583]
77. Li Y, Yang W, Wang HC, Patel RM, Casey EB, Denby E, and Magee JA (2023). Basal type I interferon signaling has only modest effects on neonatal and juvenile hematopoiesis. Blood Adv. 7, 2609–2621. 10.1182/bloodadvances.2022008595. [PubMed: 36724510]
78. Porter SN, Cluster AS, Yang W, Busken KA, Patel RM, Ryoo J, and Magee JA (2016). Fetal and neonatal hematopoietic progenitors are functionally and transcriptionally resistant to Flt3-ITD mutations. Elife 5, e18882. 10.7554/eLife.18882. [PubMed: 27879203]
79. Li Y, Yang W, Patel RM, Casey EB, Denby E, Mendoza-Castrejon J, Rodriguez-Lopez P, and Magee JA (2023). FLT3ITD drives context-specific changes in cell identity and variable interferon dependence during AML initiation. Blood 141, 1442–1456. 10.1182/blood.2022016889. [PubMed: 36395068]
80. Cho YW, Hong T, Hong S, Guo H, Yu H, Kim D, Guszczynski T, Dressler GR, Copeland TD, Kalkum M, and Ge K (2007). PTIP associates with MLL3- and MLL4-containing histone H3 lysine 4 methyltransferase complex. J. Biol. Chem. 282, 20395–20406. 10.1074/jbc.M701574200. [PubMed: 17500065]
81. Zhang Y, Liu T, Meyer CA, Eeckhoute J, Johnson DS, Bernstein BE, Nusbaum C, Myers RM, Brown M, Li W, and Liu XS (2008). Model-based analysis of ChIP-Seq (MACS). Genome Biol. 9, R137. 10.1186/gb-2008-9-9-r137. [PubMed: 18798982]
82. Zhou X, Lowdon RF, Li D, Lawson HA, Madden PA, Costello JF, and Wang T (2013). Exploring long-range genome interactions using the WashU Epigenome Browser. Nat. Methods 10, 375–376. 10.1038/nmeth.2440. [PubMed: 23629413]

## Highlights

- Mono- and biallelic *Kmt2c* deletions enhance G-CSF-stimulated HSC mobilization
- *Kmt2c* deletions amplify granulocyte production from granulocyte-monocyte progenitors
- *Kmt2c* deletion enhances H3K27ac at genes associated with self-renewal and granulopoiesis
- *Kmt2c* exerts methyltransferase-independent regulation of HSC function and G-CSF sensitivity

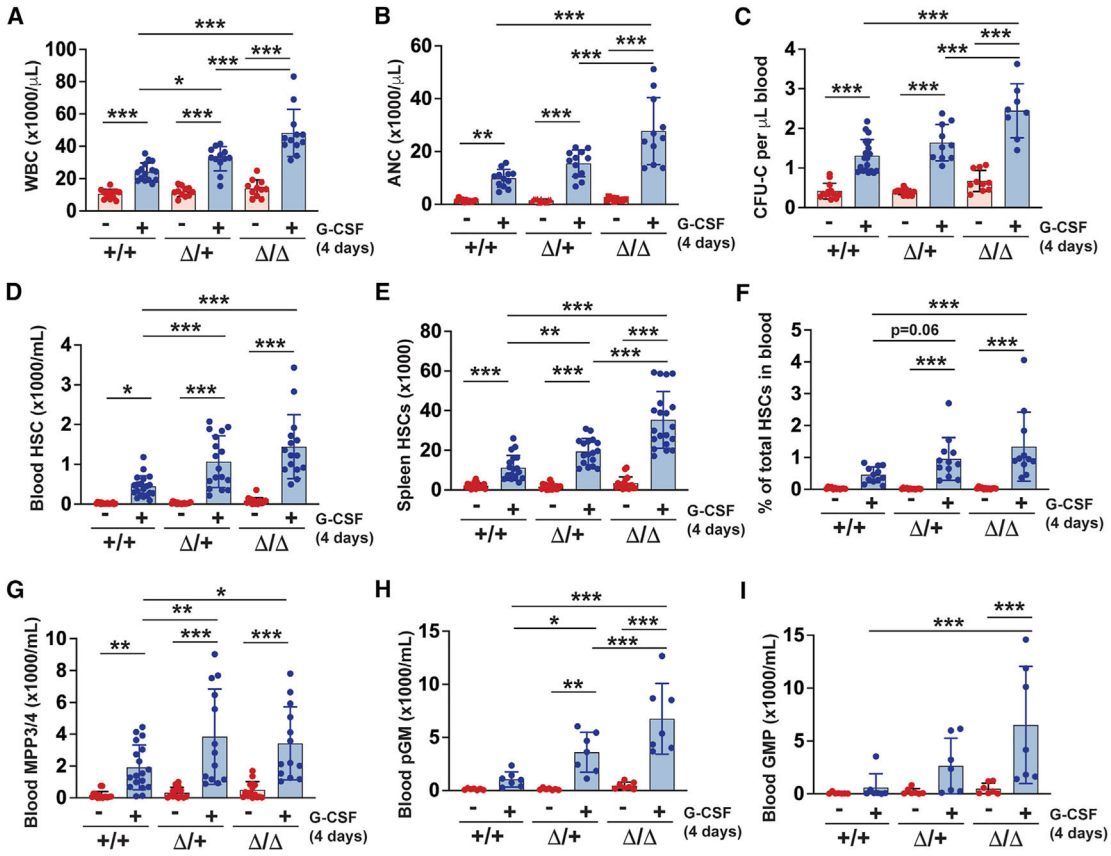


**Figure 1. Mono- and bi-allelic *Kmt2c* deletions enhance HSC and myeloid progenitor mobilization in response to G-CSF**

(A and B) Peripheral WBC and ANC values in mice of the indicated *Kmt2c* genotypes after 4 days of PBS or G-CSF treatment ($n = 12–15$).

(C) CFU-C per microliter of blood after 4 days of PBS or G-CSF treatment ($n = 11–12$).

(D and E) Peripheral blood (D) and spleen (E) HSCs after G-CSF treatment ($n = 15–20$).

(F) Peripheral blood HSCs in PBS- and G-CSF-treated mice as a percentage of total body HSCs (bone marrow + blood + spleen). The total HSC values were calculated under the assumption that two hindlimbs account for 15% of total bone marrow and that there are 3 mL of peripheral blood in an adult mouse ($n = 11–12$).

(G–I) MPP3/4 ($n = 15–18$) (G), pGM ($n = 7$) (H), and GMP ($n = 7$) (I) numbers in peripheral blood of PBS- and G-CSF-treated mice.

For all panels, error bars reflect SD; *$p < 0.05$, **$p < 0.01$, ***$p < 0.001$, as calculated by one-way ANOVA followed by Holm-Sidak post hoc test.

See also Figures S1–S4.

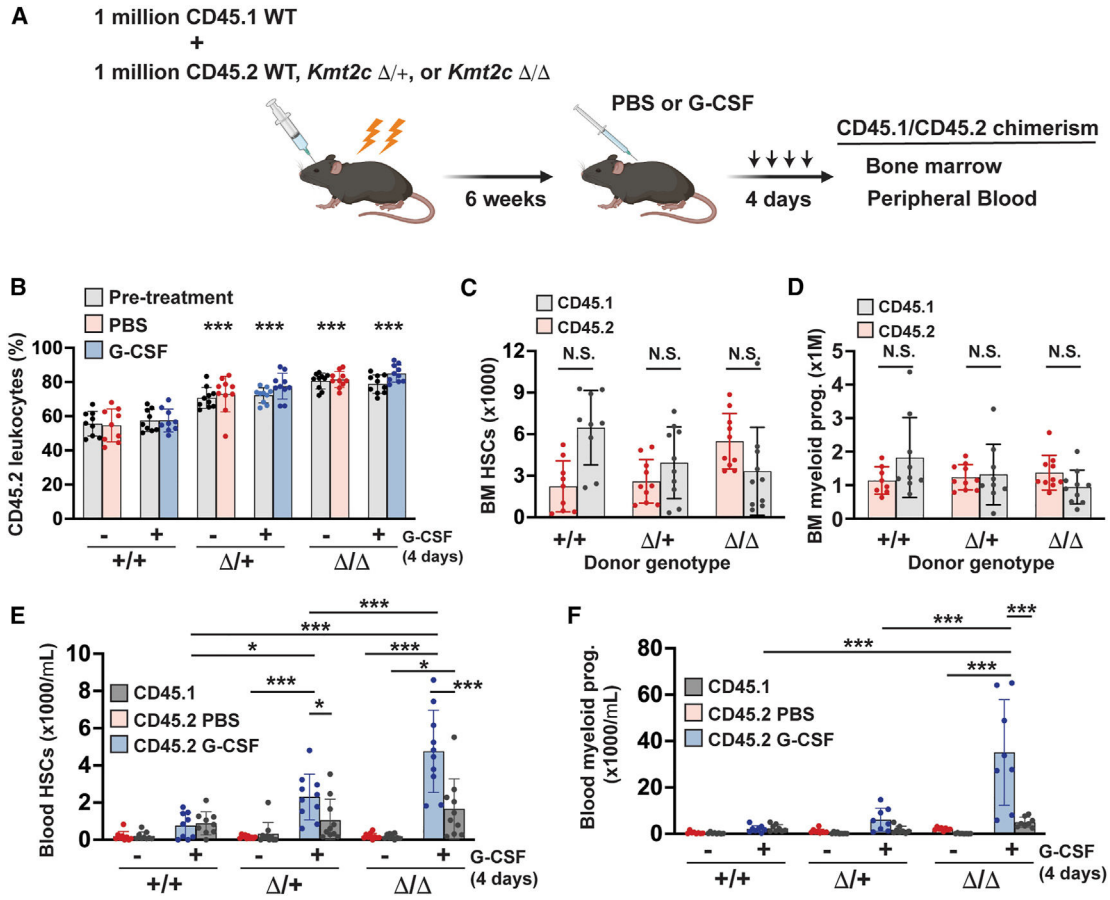


**Figure 2. *Kmt2c* cell autonomously suppresses HSC mobilization**

(A) Schematic overview of mixed chimerism experiment to test whether effects of *Kmt2c* deletion on HSC mobilization are cell autonomous or non-cell autonomous.

(B) Peripheral blood chimerism ($CD45.2^+$ blood cells as a percentage of all $CD45^+$ blood cells) in mice of the indicated genotype, before and after treatment with PBS or G-CSF ($n$ = 9–10). Statistical arguments describe the significance of the indicated *Kmt2c* genotype and treatment relative to the corresponding wild-type treatment conditions.

(C and D) Donor ($CD45.2^+$) and recipient ($CD45.1^+$) HSC (C) and myeloid progenitor ($Lineage^-Sca1^-Kit^+$) (D) numbers in the bone marrow of recipient mice after PBS treatment. The data show that $CD45.2^+$ and $CD45.1^+$ HSC populations are similar in size prior to G-CSF treatment, even in recipients of $Kmt2c^{\Delta/+}$ and $Kmt2c^{\Delta/\Delta}$ bone marrow. $CD45.2^+$ and $CD45.1^+$ myeloid progenitor populations are also similar in size ($n$ = 8–10). N.S., not significant.

(E and F) Absolute HSC and myeloid progenitor numbers in the peripheral blood of mixed chimeric mice of the indicated genotype after 4 days of PBS or G-CSF treatment ($n$ = 8–10). For all panels, error bars reflect SD; $*p < 0.05$, $**p < 0.01$, $***p < 0.001$, as calculated by one-way ANOVA followed by Holm-Sidak post hoc test.

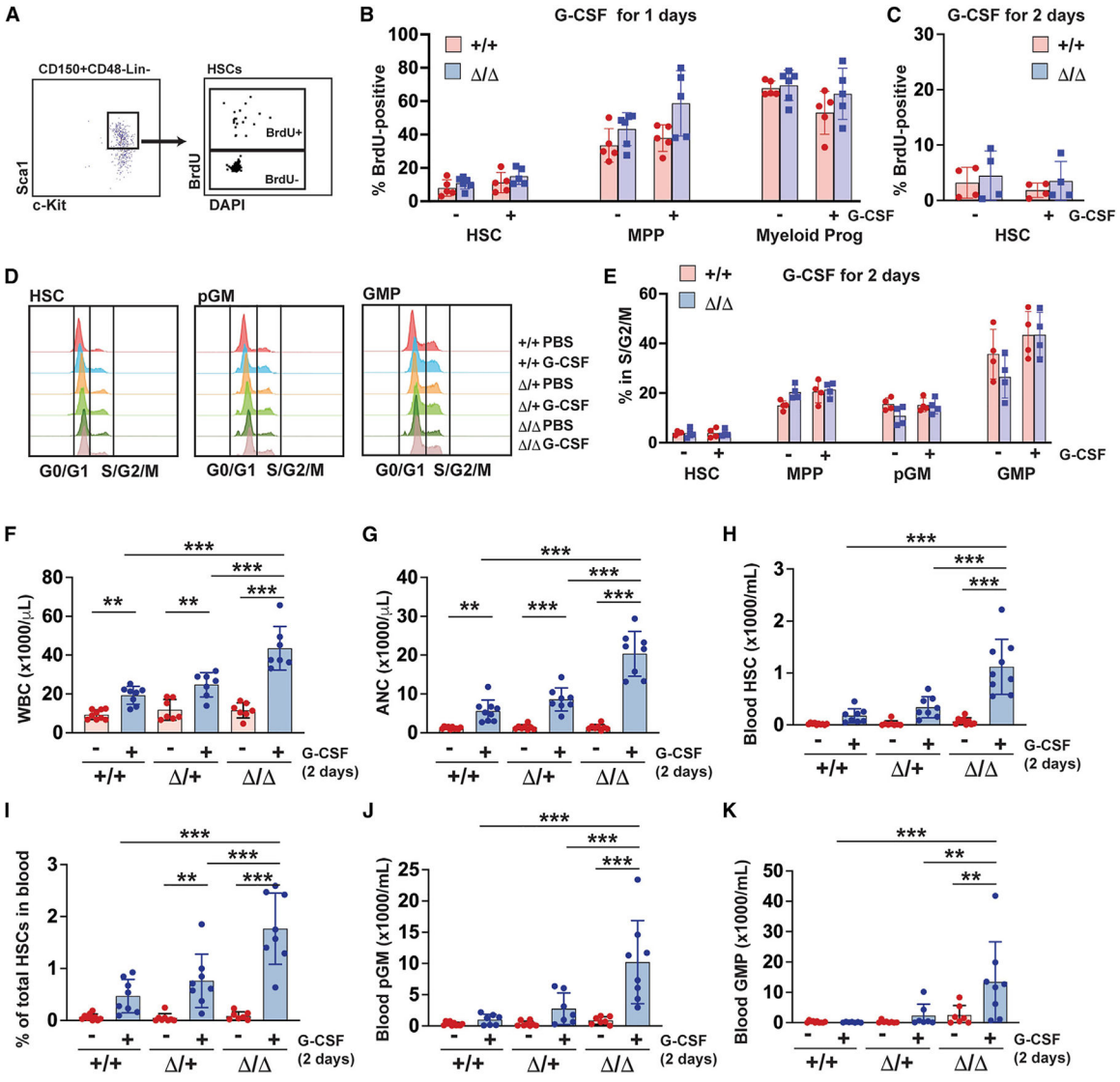


**Figure 3. *Kmt2c* deletion enables rapid mobilization of HSCs and myeloid progenitors without altering proliferation rates**

(A) Representative flow cytometry plot for BrdU analyses.

(B and C) Percent of BrdU$^{+}$ progenitors in the bone marrow of *Kmt2c*$^{+/+}$ and *Kmt2c*$^{\Delta/\Delta}$ mice after 1 or 2 days of G-CSF treatment ($n$ = 4–6).

(D) Representative flow cytometry plots for propidium iodide stains of HSC, pGM, and GMP cells.

(E) Percentage of HSC, MPP, pGM, and GMP in S/G2/M phase of the cell cycle after 2 days of G-CSF treatment ($n$ = 4).

(F and G) Peripheral WBC (F) and ANC (G) values in mice of the indicated *Kmt2c* genotypes after 2 days of PBS or G-CSF treatment ($n$ = 7–9).

(H) Peripheral blood HSC numbers after 2 days of G-CSF treatment ($n$ = 8–10).

(I) Peripheral blood HSCs in control and G-CSF-treated mice as a percentage of total body HSCs (bone marrow + blood + spleen) ($n$ = 7–10).

(J and K) pGM (J) and GMP (K) numbers in peripheral blood of PBS- and G-CSF-treated mice ($n = 7–10$).

Error bars reflect SD; *$p < 0.05$, **$p < 0.01$, ***$p < 0.001$, as calculated by one-way ANOVA followed by Holm-Sidak post hoc test.

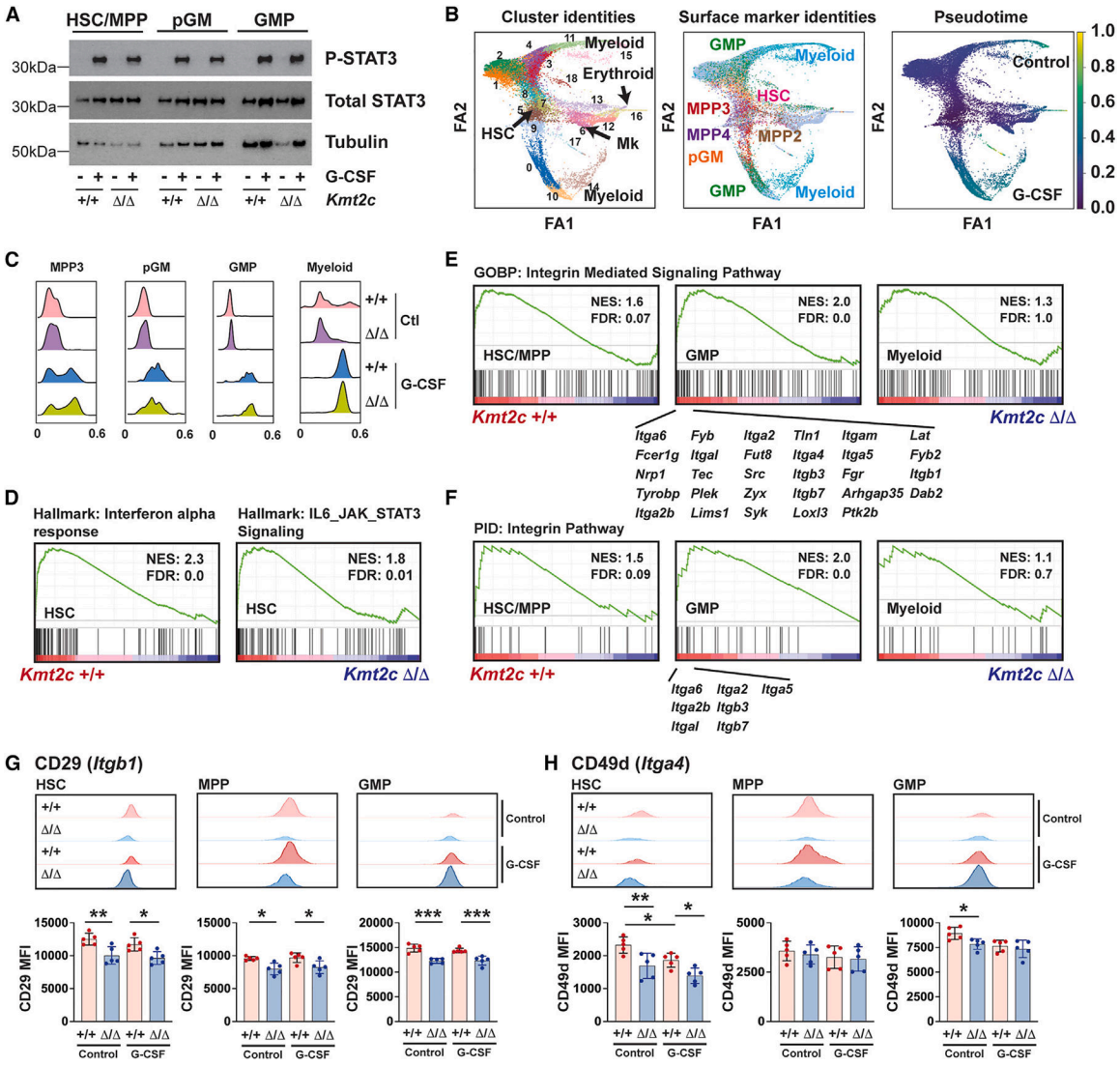


**Figure 4. *Kmt2c* deficiency does not alter signal transduction or the global differentiation trajectories of G-CSF-treated progenitors**

(A) Western blot showing STAT3 phosphorylation in HSC/MPP, pGM, and GMP cells of the indicated *Kmt2c* genotypes after G-CSF stimulation.

(B) Force-directed graphs representing single-cell transcriptomes of Ter119$^{-}$B220$^{-}$CD3$^{-}$Kit$^{+}$ cells from the bone marrow of *Kmt2c*$^{+/+}$ and *Kmt2c*$^{\Delta/\Delta}$ mice after 2 days of G-CSF treatment. (Left) Cluster assignments by Louvain clustering. Cluster identities are indicated based on the expression of canonical marker genes (see Figure S5B). (Center) Populations based on the expression of surface markers, as measured by CITE-seq. (Right) Pseudotime differentiation states.

(C) Quantification of pseudotime differentiation states for cells in each indicated genotype, treatment group, and progenitor population. G-CSF treatment resulted in qualitatively greater degrees of differentiation in each population, irrespective of *Kmt2c* genotype.

(D) GSEA plots for hallmark interferon and inflammatory target genes sets as calculated by pseudobulk gene expression analysis of *Kmt2c*$^{+/+}$ and *Kmt2c*$^{\Delta/\Delta}$ HSCs. The plots compare

expression in G-CSF-treated HSCs and show downregulation of these genes in *Kmt2c*$^{\Delta/\Delta}$ HSCs.

(E and F) GSEA showing downregulation of integrin-mediated signaling pathway (E) and integrin pathway (F) gene sets in G-CSF-treated *Kmt2c*$^{\Delta/\Delta}$ HSCs and GMPs. Significant differences were not evident in CD11b$^{+}$Gr1$^{+}$ myeloid progenitors. Enriched genes are indicated below the plots for each gene set.

(G and H) Flow cytometry confirming decreased surface protein expression of CD29/*Itgb1* (G) and CD49d/*Itga4* (H), in control and G-CSF-treated *Kmt2c*$^{\Delta/\Delta}$ HSCs, MPPs, and GMPs relative to wild-type progenitors. Representative flow cytometry plots are shown at the top of each panel, and mean fluorescence indices are shown in the bar graphs below ($n$ = 4–5). Error bars reflect SD; *$p < 0.05$, **$p < 0.01$, ***$p < 0.001$, as calculated by one-way ANOVA followed by Holm-Sidak post hoc test.

See also Figures S5–S7.

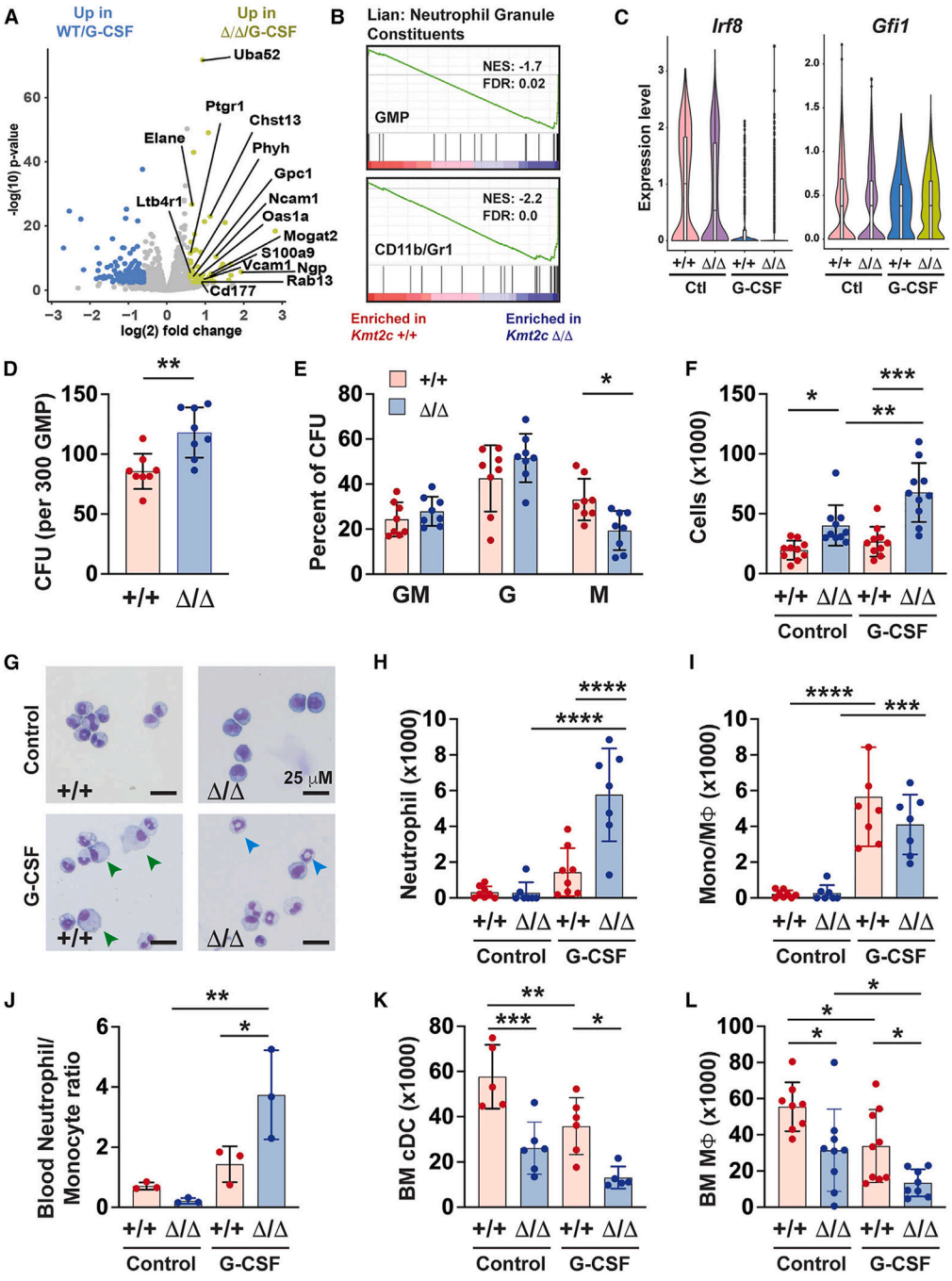


**Figure 5. *Kmt2c* deficiency amplifies granulocyte production from GMPs**

(A) Volcano plot showing differentially expressed genes between G-CSF-stimulated *Kmt2c*$^{+/+}$ and *Kmt2c*$^{\Delta/\Delta}$ GMPs, based on pseudobulk analysis of the CITE-seq data in Figure 4. Several genes associated with neutrophil identity are indicated on the volcano plot and are more highly expressed in *Kmt2c*$^{\Delta/\Delta}$ GMPs.

(B) GSEA demonstrating enrichment for neutrophil-associated genes in G-CSF-stimulated, *Kmt2c*$^{\Delta/\Delta}$ GMPs, and CD11b$^{+}$/Gr1$^{+}$ myeloid progenitors.

(C) *Irf8* and *Gfi1* are expressed at comparable levels in *Kmt2c*$^{+/+}$ and *Kmt2c*$^{\Delta/\Delta}$ GMPs.

(D) CFU observed after plating 300 *Kmt2c*$^{+/+}$ or *Kmt2c*$^{\Delta/\Delta}$ GMPs into MethoCult ($n$ = 8).
(E) Morphologic assessment of GMP colonies revealed modest reduction in monocytic CFU-M and a corresponding but not significant increase in CFU-G ($n$ = 8).
(F) Total cell numbers after 1,000 GMPs of the indicated *Kmt2c* genotype were cultured for 5 days, with or without G-CSF (1 ng/mL) ($n$ = 12).
(G) Representative cytospin pictures demonstrating cell morphology after GMPs were cultured with or without G-CSF. Cells with mature monocytic/macrophage morphology are noted with green arrowheads. Cells with mature neutrophil morphology are noted with blue arrowheads. Scale bars, 25 μm.
(H and I) Number of cultured cells with mature neutrophil (H) or monocyte/macrophage
(I) morphology. Values were calculated by multiplying the fraction of cells with neutrophil or monocyte/macrophage morphology on cytospin analysis by the total cell number in each culture ($n$ = 7–8).
(J) Peripheral blood neutrophil-to-monocyte ratios after *Kmt2c*$^{+/+}$ or *Kmt2c*$^{\Delta/\Delta}$ mice were treated with G-CSF for 4 days. Representative flow cytometry plots are shown in Figure S9D. ($n$ = 3).
(K and L) Bone marrow classical DC (cDC) ($n$ = 5–6) and macrophage (MΦ) ($n$ = 9–10) numbers in *Kmt2c*$^{+/+}$ or *Kmt2c*$^{\Delta/\Delta}$ mice after 4 days of G-CSF treatment. Representative flow cytometry plots are shown in Figures S9E and S9F.
Error bars reflect SD; *$p$ < 0.05, **$p$ < 0.01, ***$p$ < 0.001, as calculated by one-way ANOVA followed by Holm-Sidak post hoc test.
See also Figures S8 and S9.

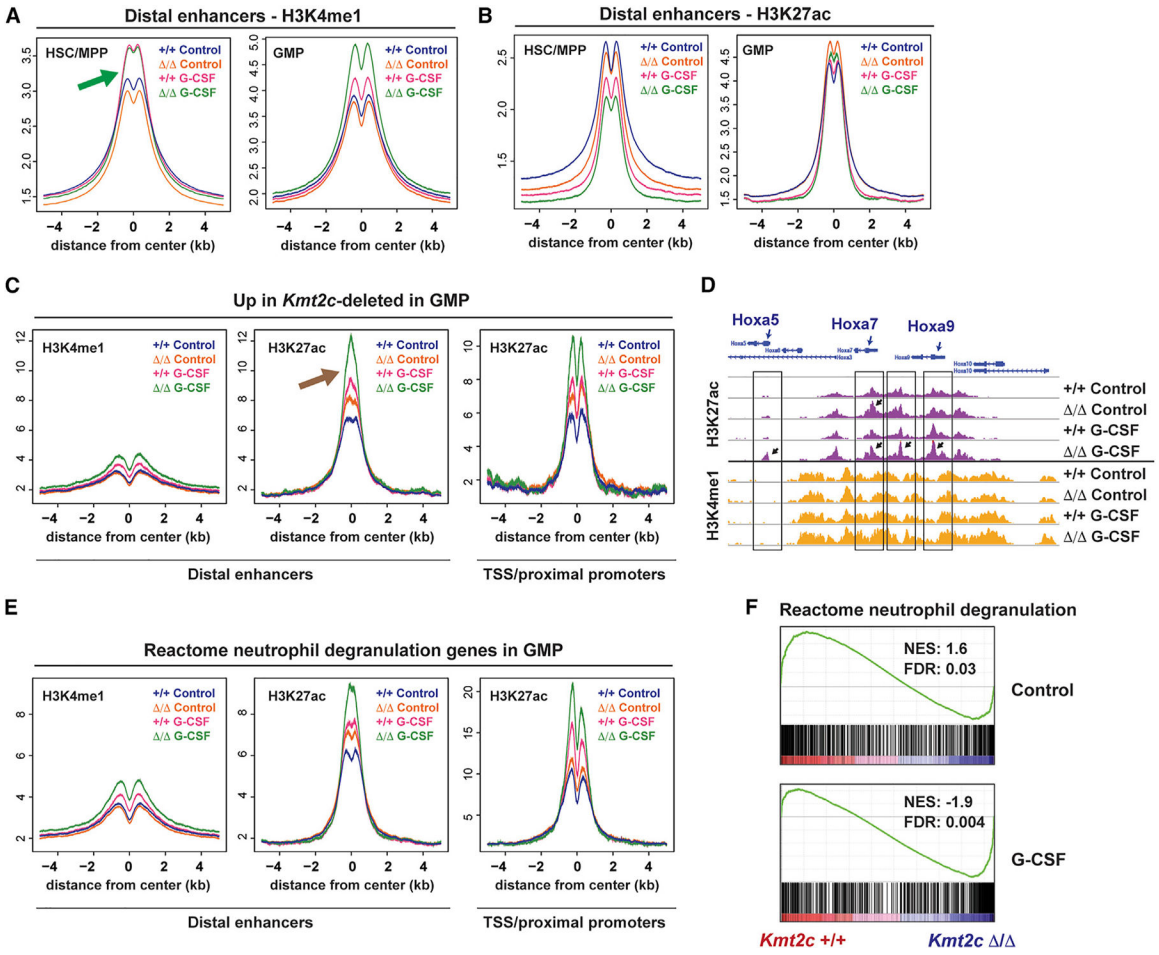


**Figure 6. MLL3 inactivation causes histone H3K27 hyperacetylation at enhancer and promoter elements of Hoxa cluster genes and neutrophil-associated genes in GMPs**

(A and B) Aggregate H3K4me1 and H3K27ac levels at distal enhancers in wild-type (+/+) and *Kmt2c*-deleted (Δ/Δ) HSC/MPPs and GMPs after 2 days of PBS or G-CSF treatment. The distal enhancers were defined as overlapping ATAC-seq and H3K4me1 peaks in each indicated cell population.

(C) H3K27ac levels at distal enhancers (within 100 kb of the gene body) and proximal promoters of genes more highly expressed in $Kmt2c^{\Delta/\Delta}$ GMPs relative to wild-type GMPs after G-CSF exposure, based on CITE-seq analyses in Figure 4 and Table S2.

(D) H3K4me1 and H3K27ac tracks at the *Hoxa* cluster. Boxes indicate elements with significant differences between wild-type and $Kmt2c^{\Delta/\Delta}$ GMPs, as calculated by diffbind. The arrows denote peaks of increased H3K27ac in $Kmt2c^{\Delta/\Delta}$ GMPs. $n$ = 3–4 biological replicates per genotype/cell type/treatment group.

(E) Increased H3K27ac levels at both distal enhancers and proximal promoters of neutrophil-associated genes in $Kmt2c^{\Delta/\Delta}$ GMPs after G-CSF exposure.

(F) GSEA showing upregulation of neutrophil-associated genes in $Kmt2c^{\Delta/\Delta}$ GMPs relative to wild-type GMPs, specifically after G-CSF treatment.

See also Figure S10.

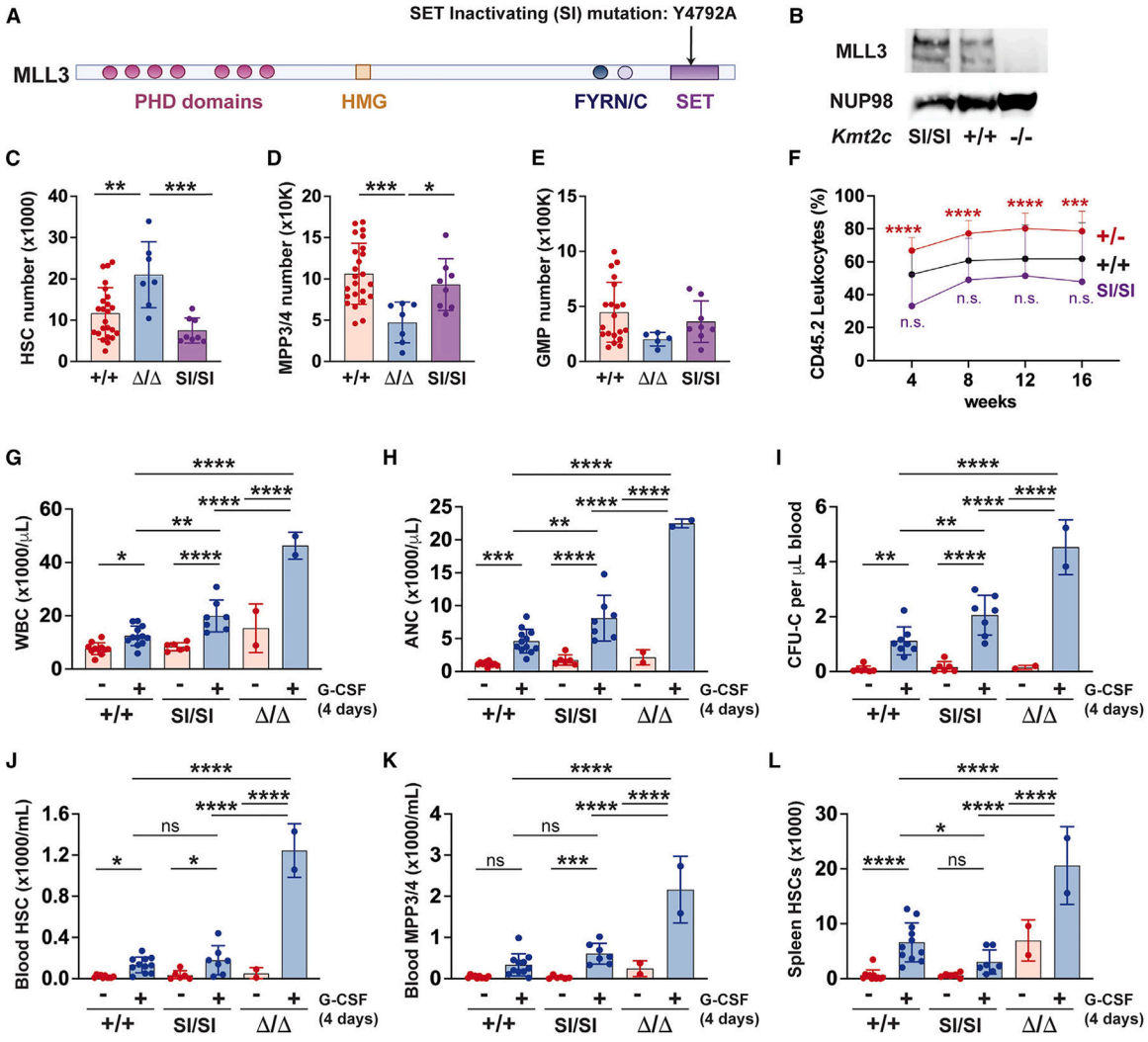


**Figure 7. Loss of MLL3 methyltransferase activity does not enhance HSC repopulating activity, HSC mobilization, or granulocyte production in response to G-CSF**

(A) Schematic of MLL3 domain structures. The arrow indicates the Y4793A mutation in the SET domain that has been previously shown to abrogate MLL3 histone methyltransferase activity.

(B) Expression of wild-type and SI MLL3 proteins in lysates from mouse embryonic fibroblasts of the indicated genotypes, as assessed by western blot. A more extended crop with the nearest molecular weight markers annotated is shown in Figure S11B.

(C–E) Numbers of HSCs (C), MPP3/4s (D), and pGMs (E) in 8-week-old adult bone marrow from mice of the indicated *Kmt2c* genotypes ($n = 4–24$).

(F) CD45.2$^+$ donor leukocyte chimerism in peripheral blood from recipients at the indicated weeks after transplantation ($n = 10–29$ recipients per donor genotype from at least 2 independent donors).

(G and H) Peripheral WBC (G) and ANC (H) values in mice of the indicated *Kmt2c* genotypes after 4 days of PBS or G-CSF treatment ($n = 2–12$).

(I) CFU-C per microliter of blood after 4 days of PBS or G-CSF treatment ($n = 2–8$).

(J and K) Peripheral blood HSC (J) and MPP3/4 (K) numbers after G-CSF treatment ($n$ = 2–12).

(L) Spleen HSC numbers after G-CSF treatment ($n$ = 2–12).

Error bars reflect SD; *$p < 0.05$, **$p < 0.01$, ***$p < 0.001$, as calculated by one-way ANOVA followed by Holm-Sidak post hoc test.

See also Figure S11.

## KEY RESOURCES TABLE

| REAGENT or RESOURCE | SOURCE | IDENTIFIER |
|---|---|---|
| Antibodies | | |
| CD150-PE | Biolegend | 115904; RRID: AB_313683 |
| CD48-PE-Cy7 | Biolegend | 103424; RRID: AB_2075049 |
| Sca1-PerCP-Cy5.5 | Biolegend | 108124; RRID: AB_893615 |
| CD2-FITC | Biolegend | 100105; RRID: AB_312652 |
| CD3-FITC | Biolegend | 100204; RRID: AB_312661 |
| CD8a-FITC | Biolegend | 100706; RRID: AB_312745 |
| B220-FITC | Biolegend | 103206; RRID: AB_312991 |
| Gr1-FITC | Biolegend | 108406; RRID: AB_313371 |
| Ter119-FITC | Biolegend | 116206; RRID: AB_313707 |
| CD105-APC | Biolegend | 120414; RRID: AB_2277914 |
| CD16/32-BV711 | Biolegend | 101337; RRID: AB_2565637 |
| CD45.1-FITC | Biolegend | 110706; RRID: AB_313494 |
| CD45.2-AF700 | Biolegend | 109822; RRID: AB_493731 |
| CD2-APC | Biolegend | 100111; RRID: AB_2563089 |
| CD3-APC | Biolegend | 100235; RRID: AB_2561455 |
| CD8a-APC | Biolegend | 100711; RRID: AB_312750 |
| B220-APC | Biolegend | 103211; RRID: AB_312996 |
| Gr1-APC | Biolegend | 108411; RRID: AB_313376 |
| Ter119-APC | Biolegend | 116211; RRID: AB_313712 |
| CD117-APC-Cy7 | Biolegend | 105826; RRID: AB_1626278 |
| CD117-Biotin | Biolegend | 135804; RRID: AB_313213 |
| CD29-FITC | Biolegend | 102205; RRID: AB_312883 |
| CD49d-FITC | Biolegend | 103605; RRID: AB_313036 |
| CD11a-FITC | Biolegend | 101106; RRID: AB_312779 |
| CD49f-FITC | Biolegend | 313605; RRID: AB_345300 |
| CD2-PE-Cy7 | Biolegend | 300221; RRID: AB_2572065 |
| CD3-PE-Cy7 | Biolegend | 100219; RRID: AB_1732068 |
| CD8a-PE-Cy7 | Biolegend | 100721; RRID: AB_312760 |
| B220-PE-Cy7 | Biolegend | 103221; RRID: AB_313004 |
| Gr1-PE-Cy7 | Biolegend | 108415; RRID: AB_313380 |
| Ter119-PE-Cy7 | Biolegend | 116223; RRID: AB_2137788 |
| CD11b-APC-Cy7 | Biolegend | 101226; RRID: AB_830642 |
| CD115-PE-Cy7 | Biolegend | 135523; RRID: AB_2566459 |
| Ly6C-PE | Biolegend | 128007; RRID: AB_1186132 |
| Ly6G-FITC | Biolegend | 127606; RRID: AB_1236488 |
| Gr1-PE | Biolegend | 108408; RRID: AB_313373 |
| B220-PerCP-Cy5.5 | Biolegend | 103236; RRID: AB_893354 |
| MHC-II-FITC | Biolegend | 107605; RRID: AB_313321 |

| REAGENT or RESOURCE | SOURCE | IDENTIFIER |
|---|---|---|
| CD169-PE-Cy7 | Biolegend | 142411; RRID: AB_2563911 |
| F4/80-APC | Biolegend | 123115; RRID: AB_893493 |
| Gr1-PE-Cy7 | Biolegend | 108416; RRID: AB_313381 |
| B220-PE | Biolegend | 103208; RRID: AB_312992 |
| CD11c-APC | Biolegend | 117309; RRID: AB_313778 |
| CD45.2-FITC | Biolegend | 109806; RRID: AB_313443 |
| CD45.1-APC-Cy7 | Biolegend | 110716; RRID: AB_313505 |
| CD3-PE | Biolegend | 100206; RRID: AB_312663 |
| CD11b-APC | Biolegend | 101212; RRID: AB_312795 |
| P-STAT3 | Cell Signaling | 9145S; RRID: AB_2491009 |
| STAT3 | Cell Signaling | 9139S; RRID: AB_331757 |
| p-S6 | Cell Signaling | 5364S; RRID: AB_10694233 |
| S6 | Cell Signaling | 2217S; RRID: AB_331355 |
| α-Tubulin | Cell Signaling | 2144S; RRID: AB_2210548 |
| NUP98 | Cell Signaling | 2288S; RRID: AB_561204 |
| MLL3 | From Kai Ge | N/A |
| H3K4me1 | Diagenode | C15410194; RRID:AB_2637078 |
| H3K27ac | Diagenode | C1541096; RRID:AB_2637079 |
| CD150 | Biolegend | 115951; RRID:AB_2860628 |
| CD48 | Biolegend | 103457; RRID:AB_2860604 |
| CD135 | Biolegend | 135319; RRID:AB_2832479 |
| CD117 | Biolegend | 105849; RRID:AB_2813938 |
| CD16/32 | Biolegend | 101345; RRID:AB_2819782 |
| CD41 | Biolegend | 133941; RRID:AB_2876468 |
| CD127 | Biolegend | 135055; RRID:AB_2860677 |
| CD34 | Biolegend | 152213; RRID:AB_2888881 |
| SA-PE | Biolegend | 405287; N/A |
| CD201 | Biolegend | 141511; RRID:AB_2894657 |
| CD11b | Biolegend | 101273; RRID:AB_2819781 |
| Gr1 | Biolegend | 108465; RRID:AB_2832372 |
| Chemicals, peptides, and recombinant proteins | | |
| Streptavidin-APC-Cy7 | Biolegend | 405208 |
| Mojosort Streptavidin Nanobeads | Biolegend | 76447 |
| G-CSF (Neupogen) | Amgen | NDC 55513-530-10 |
| Plerixafor | Adooq bioscience | A13074 |
| Bromodeoxyuridine | Sigma-Aldrich | B5002 |
| Recombinant murine TPO | Peprotech | 315–14 |
| Recombinant murine SCF | Peprotech | 250–03 |
| MethoCult™ GF M3434 | Stem cell technologies | 03434 |
| StemSpan™ SFEM II | Stem cell technologies | 09650 |
| DirectPCR lysis reagent (Mouse Tail) | Viagen | 101-T |

| REAGENT or RESOURCE | SOURCE | IDENTIFIER |
|---|---|---|
| NuPAGETM LDS Sample Buffer (4X) | Thermo Fisher Scientific | NP0007 |
| SuperSignal™ West Pico PLUS Chemiluminescent Substrate | Thermo Fisher Scientific | 34577 |
| SuperSignal™ West Femto Maximum sensitivity Thermo Fisher Scientific 34095 Substrate | Thermo Fisher Scientific | 34095 |
| Critical commercial assays | | |
| APC BrdU Flow Kit | BD | 51–9000019AK |
| Ampure XP SPRI Beads | Beckman | B23318 |
| NuPage™ 4 to 12% Bis-Tris Gel | Thermo Fisher Scientific | NP0335PK2 |
| NuPage™ 3 to 8% Tris-Acetate Gel | Thermo Fisher Scientific | EA0375BOX |
| Chromium Single Cell 3' Library and Gel Bead Kit v2 | 10x Genomics | PN-120237 |
| Chromium Single Cell 3' Chip kit v2 | 10x Genomics | PN-120236 |
| Chromium i7 Multiplex Kit | 10x Genomics | PN-120262 |
| Deposited data | | |
| scRNA-seq, ATAC-seq, Chipmentation | This paper | GEO: GSE243869 |
| Experimental models: Organisms/strains | | |
| Mouse: C57BL/6J | The Jackson Laboratory | RRID:IMSR_JAX:006965 |
| Mouse: B6.Cg-*Commd10*$^{Tg(Vav1\text{-}icre)A2Kio}$/J | The Jackson Laboratory | RRID:IMSR_JAX:008610 |
| Mouse: B6.129P2-*Lyz2*$^{tm1(cre)Ifo}$/J | The Jackson Laboratory | RRID:IMSR_JAX:004781 |
| Mouse: B6(Cg)-*Kmt2c*$^{em1Mgee}$/J | Chen et al.[31] | RRID:IMSR_JAX:037115 |
| Mouse: B6(Cg)-*Ifnar1*$^{tm1.2Ees}$/J | The Jackson Laboratory | RRID:IMSR_JAX:028288 |
| Mouse: *Kmt2c*$^{SI}$ | This study | N/A |
| Oligonucleotides | | |
| Primer for the exon 3 conditional floxed allele genotyping: Forward: GAACCTGAGGCTGTCGAAGG | Chen et al.[31] | N/A |
| Primer for the exon 3 conditional floxed allele genotyping: Reverse: AGCCATTAAACTTAGTGAAGACCA | Chen et al. [31] | N/A |
| Primer for the exon 3 conditional to identify deleted allele: Forward: GCTCCTCCTCTGGCTTCCAAGGTCA | Chen et al.[31] | N/A |
| Primer for the exon 3 conditional to identify deleted allele: Reverse: AGGGCATCTAATCTGACAGCTGTAAGC | Chen et al.[31] | N/A |
| Primer for the SET inactivating allele genotyping: Forward (common): ttggagtgcttgttacgctg | This study | N/A |
| Primer for the SET inactivating allele genotyping: Reverse (wildtype): cgaataattgttccaatgtactcg | This study | N/A |
| Primer for the SET inactivating allele genotyping: Reverse (mutant): cgaataatAgttccGatGGC | This study | N/A |
| Software and algorithms | | |
| RStudio | RStudio | https://rstudio.com |
| Seurat v3 | Butler et al.,[68] Stuart et al.[69] | https://satijalab.org/seurat/ |

| REAGENT or RESOURCE | SOURCE | IDENTIFIER |
|---|---|---|
| CellRanger v2.1.0/v3.0.1 | 10x Genomics | https://support.10xgenomics.com/single-cell-gene-expression/software/overview/welcome |
| DESeq2 | Love et al.[70] | https://bioconductor.org/packages/release/bioc/html/DESeq2.html |
| Gene Set Enrichment Analysis (GSEA) | Subramanian et al.[71] | https://www.gsea-msigdb.org/gsea/index.jsp |
| Presto | Korsunsky et al.[72] | N/A |
| Scanpy | Wolf et al.[47] | https://scanpy.readthedocs.io/en/stable/ |
| PAGA | Wolf et al.[47] | https://github.com/theislab/paga |
| ATAC-seq processing pipeline, v0.3.3 | Corces et al.[73] | https://github.com/kundajelab/atac_dnase_pipelines |
| Bowtie2 | Bowtie, v2.2.26 | http://bowtie-bio.sourceforge.net/bowtie2/index.shtml |
| DiffBind | DiffBind | http://www.bioconductor.org/packages/2.13/bioc/html/DiffBind.html |
| Irreproducible Discovery Rate (IDR) | Li et al.[74] | https://www.encodeproject.org/software/idr |
| MACS2 | MACS2, V2.1.0 | https://github.com/macs3-project/MACS |
| BD FACSDiva | BD | N/A |
| Flowjo v.10 | Treestar | N/A |
| Prism v.10 | GraphPad | N/A |
| WashU Epigenome browser | Roadmap Epigenomics[75] | https://epigenomegateway.wustl.edu |